Structural vs. Chemical: A Statistical Approach to the Multimodal Correlation Structure of the Human Brain

Kevin Souder kesouder@ucsd.edu
Kevin Huang tih009@ucsd.edu
Armin Schwartzman armins@ucsd.edu
Gabriel Riegner gariegner@ucsd.edu

Abstract

The human brain is organized across multiple interacting biological layers, two major components are structural and functional layers. While these modalities are often studied independently, understanding how they covary is important for characterizing large-scale principles of cortical organization. In this project, we investigate the multimodal covariance structure of the human cortex by integrating eight widely used structural and functional brain maps into a unified statistical framework. Using data standardized through the neuromaps pipeline, we construct an all-to-all multimodal correlation matrix capturing pairwise relationships between brain maps. To ensure valid inference accounting spatial autocorrelation, statistical significance is assessed using spatial spin tests combined with spin-based Max-T correction and complementary multiple-comparison procedures. We further examine the low-dimensional organization of this covariance structure using principal component analysis and evaluate coherence within and between hypothesized structural and neurochemical modes via subgroup connectivity analysis. Together, these approaches allow us to test whether brain organization is best described by partially segregated structural and chemical systems or by more integrated multimodal relationships. Our results provide a statistically robust characterization of multimodal cortical organization and establish a generalizable framework for future studies linking brain structure, neurochemistry, and function, with potential implications for understanding neuropsychiatric disorders characterized by structural–functional decoupling.

Website: https://kevinhuang8706.github.io/dsc_capstone_website/
Code: https://github.com/kesouder/BrainMap_Analysis

1 Introduction

1.1 Context

The human brain functions as an intricate system composed of distinct biological layers. These consist of the physical and structural (e.g. myelin ratio and cortical thickness), and chemical and functional (e.g. glucose metabolism and 5-HT1a receptors) layers. To better understand this system, we can think of the brain as a city with roads and traffic. The roads allow for cars to travel in the city, similar to the structure of the brain allowing neural signals to travel throughout the brain. The traffic pattern represents the functional activity within the brain. For example, think of the chemical functionality as a red light. The road could be open, but cars cannot move until the light turns green. Similarly to the brain, regardless of whether the structure is healthy, the chemical and functional layers of the brain are ultimately what controls information flow throughout the brain.

Current neuroscience often studies these components in isolation, overlooking their critical interactions. Furthermore, standard statistical methods fail due to spatial autocorrelation, the idea that neighboring regions are more similar than regions further away, which violates the independence assumptions and causes an inflation of false positive. To address this, we employ the spin test (Alexander-Bloch et al. 2018) developed by Alexander Bloch et al. This spatial null model generates brain maps by rotating the cortical surface on a sphere, preserving the intrinsic spatial topology of the original data while randomizing the alignment between maps. Alignment in the scope of this project means that every spot on the brain has two paired measurements, one from brain map A and one from brain map B, that are lined up for direct comparison. This rigorous framework allows us to confidently distinguish true biological coupling from random spatial coincidence, providing a reliable foundation for characterizing the interplay between the brain's physical and functional layers.

1.2 Our Project

To implement this rigorous framework, we use the neuromaps library and toolbox that includes a variety of brain images and functions to transform and compare different brain images (Markello et al. 2022, 2024). This toolbox allows us to integrate structural MRI brain maps with neurochemical brain maps derived from PET and fMRI readings into one library for analysis and plotting. By transforming these two imaging layers (surface versus volumetric brain maps) onto a common cortical surface, we can quantify the spatial correlation between the brain's structural components and dynamic signaling properties. Our Quarter 2 project aims to address and analyze the gap between structural and neurochemical layers of the brain by creating a comprehensive Multimodal Correlation Matrix that simultaneously compares structural, functional, and chemical brain maps to reveal the brain's unified complex layout. We hypothesize that the brain's correlation structure is characterized by distinct segregated modes: structural and neurochemical. This matrix will quantify the correlation between different layers of the brain, allowing us to conclude if

they operate as distinct systems. The brain maps we will use for our hypothesis include the structural brain maps: PC1 Gene Expression (Markello et al. 2021), Myelin ratio and Cortical Thickness (Glasser et al. 2016), and Allometric Scaling (NIH) (Reardon et al. 2018), and the chemical/functional brain maps: Functional Gradient (Margulies et al. 2016), Glucose Metabolism (Vaishnavi et al. 2010), Intersubject Variability (Mueller et al. 2013), and 5-HT1a Receptor (Savli et al. 2012). To visualize these relationships, we will employ density scatter plots using the raw brain map data as well as ranked density scatter plots to visualize global correlations between map pairs under the Spearman correlation ρ. Furthermore, we will investigate the spatial tethering of these signals by generating local coupling maps, which will reveal and help visualize how the alignment between structural and neurochemical layers varies across brain regions. Continuing with our analytical pipeline, we will implement significance testing and multiple test correction methods to correct for the inflated number false positives. Within the scope of this project, we aim to bridge the gap between physical anatomy and neurochemical function by establishing a normative baseline for the brain's organization. By establishing this multimodal correlation structure, we create a robust statistical framework for investigating this disconnect between the physical and chemical layers of the brain. This is vital for further exploration and validation of the potential relationships between physical brain anatomy and fundamental cognitive dynamics.

2 Methods

2.1 Data Pre-Processing

We started our analytical pipeline by accessing the neuromaps toolbox (Markello et al. 2022) to fetch and load all the brain map files needed. Using the provided neuromaps framework and functions, we retrieved the file paths for each brain map and then loaded the surface data (vertices) from the neuromaps atlas (Robinson et al. 2014, 2018), as well as the volumetric data for the 5-HT1a Receptor brain map. We transformed the 5-HT1a brain map from volumetric space MNI-152 to surface space fsLR density 32k (Buckner et al. 2011; Wu et al. 2018) via neuromap's built in transform function. We created global dictionaries including the needed arguments to fetch the data (source, description, space, and density), and another for readable names of each brain map for all figures and tables throughout our project. For efficiency, we created a function to load and transform our brain map data which standardized all our brain maps to a common space and coordinate system fsLR at a 32k density. This function uses the global dictionaries to fetch the needed arguments, handles transformations, spatially resamples the data points (vertices), and finally outputs a single array that ensures the vertex-wise alignment across all brain maps for our multimodal correlation analysis. We then wrote a function to plot all 8 brain maps using Python's Matplotlib (Hunter 2007). Keeping in mind that the 5-HT1a Receptor brain map needs to be transformed prior to plotting, we incorporated a conditional statement for this case in which we transformed the brain map so the plotting functionality works with the other brain maps. We created another dictionary specifically for this function to specify

brain map color and the data range. In order to create the most representative brain map, we displayed both hemispheres with a corresponding color bar to show the range of values for the respective brain map.

2.2 Multimodal Correlation Matrix

We first assessed the relationships between eight brain maps (28 unique pairs) using Pearson (r) and Spearman (ρ) correlations to identify linear versus non-linear associations. Given the high dimensionality (about $32,000$ vertices) of our data, we visualized raw data distributions using hexbin density scatter plots. To account for the predominantly non-linear and monotonic trends, we generated a second set of plots using rank-transformed data (utilizing Python numpy's rankdata functionality (Virtanen et al. 2020). This transformation linearizes monotonic relationships by comparing relative ranked order instead of raw values, converting curved trends into linear diagonal associations. For both of these plots, we produced 28 subplots that showed the relationship between brain map pairs as well as added more insight to our hypothesis regarding the global strength and direction of the relationship between structural and neurochemical brain maps, quantified by the Spearman correlation coefficient (ρ).

For additional insights, we wanted to visualize on the brain regions where brain map pairs have a linear relationship (e.g. PC1 Gene Expression and T1W/T2W Ratio), complex relationship (e.g. T1W/T2W Ratio vs Functional Gradient), or no relationship (e.g. Allometric Scaling NIH and Glucose Metabolism). To visualize spatial differences in these relationships, we developed a brain map coupling function. Raw data were transformed into percentile ranks, and vertex wise absolute differences were calculated to generate "coupling scores." These maps identify specific regions where pairs are strongly coupled (low difference, darker areas) or decoupled (high difference, lighter areas). Finally, we constructed an 8×8 multimodal correlation matrix to provide a global overview of the Spearman ρ associations, using the color scale to represent the sign and magnitude of each relationship (positively correlated pairs in blue, negatively correlated pairs in red, and white for no relationship).

To validate these correlations, we addressed the multiple comparisons problem inherent in running 28 simultaneous tests. We applied False Discovery Rate (FDR) corrections (Benjamini-Hochberg BH (Benjamini and Hochberg 1995) and Benjamini-Yekutieli BY (White, van der Ende and Nichols 2019)) as well as the conservative Bonferroni method (Sedgwick 2012) to control for Type I Errors (false positives). Additionally, we implemented Max-T permutation testing (Oakes et al. 2005) to empirically establish significance thresholds. The Max-T Correction method is unique for this project in that it empirically models the joint distribution of test statistics to capture the spatial dependencies between vertices, unlike FDR-BH and FDR-BY which operate on p-values under generalized assumptions of dependence. Max-T provides strict Family Wise Error Rate (FWER) control that is specifically calculated for the biological smoothness of the brain imaging data and is a more rigorous validation method than the FDR methods and Bonferroni Correction. Finally, we outputted summary tables to show significant pairs under each method.

2.3 Principal Component Analysis

To characterize the dominant low-dimensional structure underlying the multimodal covariance between brain maps, we performed Principal Component Analysis (PCA) on the multimodal correlation matrix. PCA is a linear dimensionality-reduction technique that identifies orthogonal axes (principal components) capturing maximal variance in multivariate data, thereby revealing latent modes of shared variation across measurements (Jolliffe 2002).

Construction of the PCA input

PCA was performed using the existing 8×8 symmetric correlation matrix summarizing pairwise associations between all brain maps computed using Spearman correlation coefficients. Spearman correlation was chosen for the PCA input to preserve non-linear covariance structure and interpretability of component loadings, consistent with findings of pairwise scatter plots and prior multimodal neuroimaging work (Burt et al. 2018; Margulies et al. 2016).

Because the correlation matrix is symmetric and positive semi-definite by construction, PCA was implemented via eigendecomposition of the matrix:

$$\mathbf{R} = \mathbf{V}\mathbf{\Lambda}\mathbf{V}^{\intercal}$$

$\mathbf{R}$ is the correlation matrix, $\mathbf{\Lambda}$ contains the eigenvalues, and $\mathbf{V}$ contains the corresponding orthonormal eigenvectors. Eigenvalues were sorted in descending order, and the proportion of variance explained by each principal component was computed as the ratio of each eigenvalue to the sum of all eigenvalues.

Loadings and interpretation Component loadings were computed as:

$$\mathbf{L} = \mathbf{V}\mathbf{\Lambda}^{\frac{1}{2}}$$

which quantify the contribution of each original brain map to each principal component. Loadings were visualized as a heatmap (PCs x brain maps) to facilitate interpretation of multimodal structure. High-magnitude positive or negative loadings indicate strong alignment between a given brain map and the corresponding component.

We focused our interpretation on the first two principal components (PC1 and PC2), which together explained the majority of variance in the correlation structure. We then examined whether structural maps (e.g., myelin ratio, cortical thickness, gene expression PC1) clustered on one component while neurochemical and functional maps (e.g., glucose metabolism, receptor density, functional gradients) loaded preferentially onto an orthogonal component. Such a pattern would indicate a partial independence between structural and neurochemical dimensions of cortical organization.

Methodological considerations

PCA was performed on the correlation matrix rather than the raw vertex-wise data to emphasize relationships between modalities rather than spatial variance within individual maps. This approach is common in multimodal neuroimaging studies aiming to identify shared organizational axes across disparate measures (Burt et al. 2018). Because PCA enforces orthogonality of components, the resulting axes should be interpreted as statistically

independent dimensions of shared variance rather than strictly independent biological processes.

We did not apply rotational methods (e.g., varimax rotation), as our primary goal was to identify dominant variance-explaining axes rather than maximize simple structure. Component retention was guided by the proportion of variance explained and inspection of the eigenvalue spectrum rather than strict application of heuristic criteria (e.g., Kaiser criterion), given the small dimensionality of the matrix and the hypothesis-driven focus on the leading components (Jolliffe 2002).

2.4 Clustering and Subgroup Connectivity Analysis

To test whether the multimodal correlation structure exhibits a "block" organization consistent with partially segregated structural and neurochemical modes, we complemented PCA with (i) hierarchical clustering of brain maps based on their inter-map similarities and (ii) subgroup connectivity summaries comparing within- versus between-group correlations.

Hierarchical clustering on correlation-derived distances

We performed agglomerative hierarchical clustering using the Spearman multimodal correlation matrix $\mathbf{R} \in \mathbb{R}^{8\times 8}$ as input. Because clustering algorithms operate on distances rather than similarities, we converted correlations to a dissimilarity matrix by subtracting an 8×8 matrix of all 1's by $\mathbf{R}$

$$\mathbf{D} = \mathbf{1} - \mathbf{R},$$

and set the diagonal to zero ($D_{ii} = 0$) to enforce zero self-distance. This transformation maps highly positively correlated map pairs to small distances and weak/negative correlations to larger distances, allowing clustering to group maps with similar cortical spatial profiles.

We then converted $\mathbf{D}$ to condensed form using `squareform` (upper triangle without the diagonal) and applied SciPy's `linkage` function with *average linkage* (UPGMA). In average linkage, the distance between two clusters A and B is defined as the mean pairwise distance between all elements across clusters:

$$d(A,B) = \frac{1}{|A||B|} \sum_{i\in A} \sum_{j\in B} D_{ij}.$$

Starting with each brain map as its own cluster, the algorithm iteratively merges the two clusters with the smallest inter-cluster distance, producing a hierarchical tree (dendrogram) that summarizes the nested grouping structure.

To obtain discrete cluster labels for downstream subgroup summaries, we "cut" the dendrogram using `fcluster` with `criterion="maxclust"` and $k = 2$, yielding a two-cluster partition. This choice was hypothesis-driven (structural vs. neurochemical) and provides a direct clustering-based test of whether the correlation structure naturally separates into two groups. Cluster assignments were stored alongside map names for interpretation and visualization.

Subgroup connectivity: within- and between-group correlation summaries

Given a partition of the 8 maps into two groups (either hypothesis-defined or clustering-derived), we quantified subgroup connectivity by summarizing the correlation strengths (i) *within* each group and (ii) *between* groups.

Let $\mathcal{G}_1$ and $\mathcal{G}_2$ be the index sets for the two groups. We computed:

$$\bar{r}_{\text{within},1} = \frac{1}{|\mathcal{G}_1|(|\mathcal{G}_1|-1)} \sum_{\substack{i\in\mathcal{G}_1 \\ j\in\mathcal{G}_1, j\neq i}} R_{ij}, \quad \bar{r}_{\text{within},2} = \frac{1}{|\mathcal{G}_2|(|\mathcal{G}_2|-1)} \sum_{\substack{i\in\mathcal{G}_2 \\ j\in\mathcal{G}_2, j\neq i}} R_{ij},$$

and the between-group mean correlation

$$\bar{r}_{\text{between}} = \frac{1}{|\mathcal{G}_1||\mathcal{G}_2|} \sum_{i\in\mathcal{G}_1} \sum_{j\in\mathcal{G}_2} R_{ij}.$$

In implementation, we computed these quantities by masking the correlation matrix into three sets of entries: within-group off-diagonal blocks for each group and the cross-group block, then averaging the corresponding correlation values. This produces a simple, interpretable summary: if the brain maps form two coherent modes, we expect $\bar{r}_{\text{within},1}$ and $\bar{r}_{\text{within},2}$ to exceed $\bar{r}_{\text{between}}$.

Interpretation and validation

Hierarchical clustering provides an unsupervised view of whether the map-to-map similarity structure supports a two-mode organization, while subgroup connectivity analysis provides a quantitative effect-size summary of segregation by comparing within- versus between-group coupling. In Results, we report (1) the dendrogram and cluster labels, and (2) the within- and between-group mean correlations (and their differences), and assess whether observed segregation aligns with the hypothesized structural versus neurochemical grouping.

3 Results

In Figure 1, we plotted the full multimodal correlation matrix to show all 28 correlation pairs. Each cell represents the Spearman Rank Correlation coefficient ρ value between two brain maps. Just as a standard correlation matrix, the diagonal cells are the self-corrections (i.e $\rho = 1$), and the off diagonal cells reflect the correlations between unique pairs. The correlation coefficients range from -1 (represented in dark red) to +1 (represented in dark blue) to show negative or positive correlations. This matrix depicts varying color shades exhibiting various correlation strengths between specific brain map pairs. The strongest positive correlation was observed between PC1 Gene Expression and the T1W/T2W Ratio ($\rho = 0.84$). The strongest negative correlations was observed between PC1 Gene Expression and 5-HT1a Receptor ($\rho = -0.69$), and similarily PC1 Gene Expression and Cortical Thickness ($\rho = -0.67$). Several brain map pairs exhibited very weak correlations (shown

by white/almost-white cells), including Allometric Scaling versus Glucose Metabolism ($\rho = -0.01$) and Functional Gradient with Glucose Metabolism ($\rho = 0.09$).

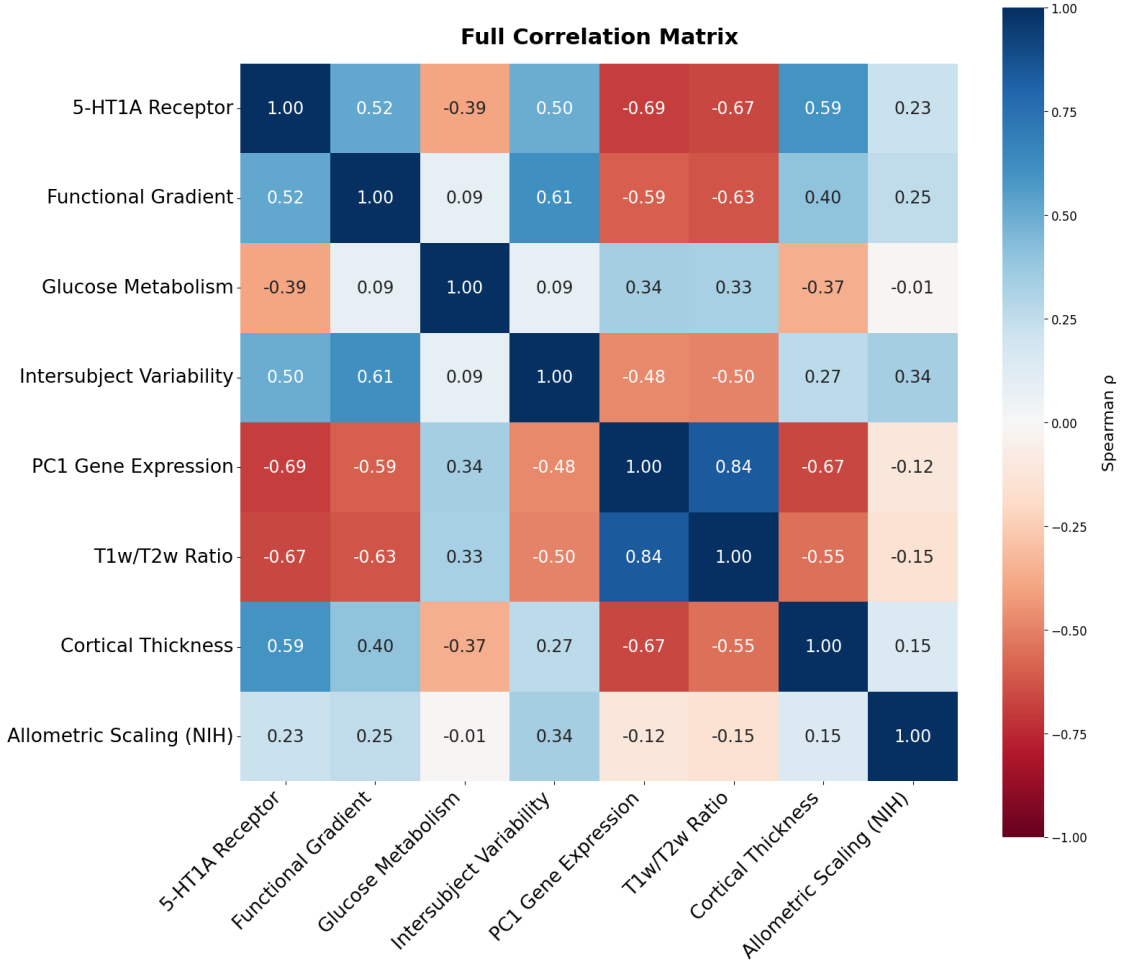

Figure 1: Spearman Correlation Matrix

Compared to the full multimodal correlation matrix using Pearson r correlation coefficient, (Figure A 10 in Appendix A.2), we overall saw that the Pearson r values were smaller than the Spearman ρ values for significant brain map pairs. We saw this with the more complex relationships such as 5-HT1a vs. Functional Gradient and Functional Gradient vs. T1W/T2W Ratio. Due to the fact that Pearson r is strictly for capturing linear relationships, utilizing Spearman ρ in this project better captures the underlying complex relationships between brain maps.

3.1 Exploratory Data Analysis

3.1.1 Pairwise Density Scatter Plot

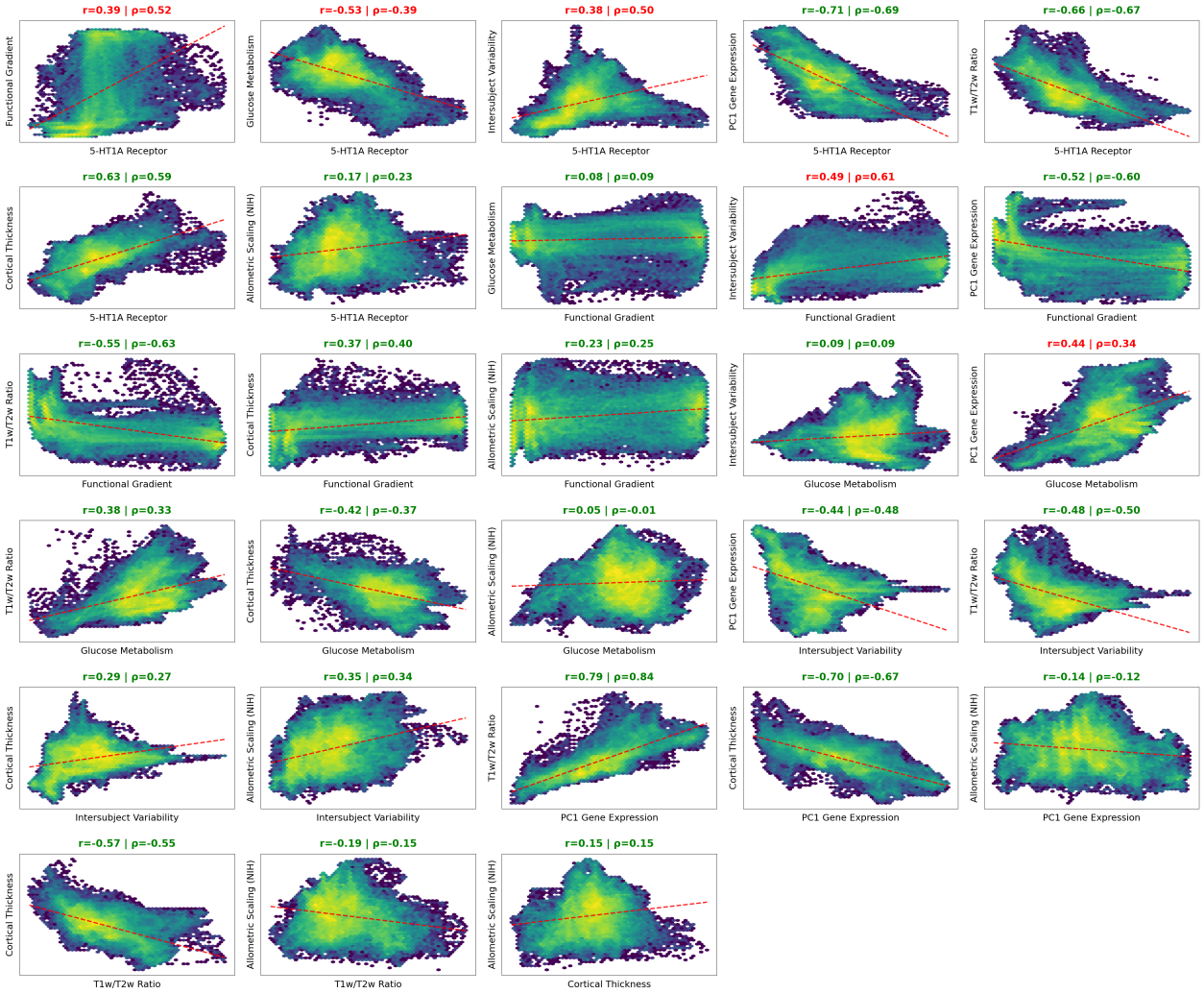

Figure 2: Pairwise Density Scatter Plots

Figure 2 displays the pairwise density scatter plot for all 28 unique brain map pairs. Each subplot displays the raw data relationship between Map A and Map B, visualized using density based binning. This plot was used to observe the linear or non-linear relationship between specific brain maps in which we displayed the Pearson r Correlation and Spearman ρ Correlation, both ranging from -1 to +1, for each subplot as well as the least squares regression lines shown for visualization purposes. We saw these subplots yield similar values between the r and ρ values, but the overall trends of the data are more complex, such as curved trends. We observe there are some linear relationships (e.g. PC1 Gene Expression with 5-HT1a Receptor, T1W/T2W Ratio, and Cortical Thickness), non-relationships (e.g. Allometric Scaling NIH with Glucose Metabolism and PC1 Gene Expression), and more complex relationships such as T1W/T2W Ratio v.s Functional Gradient and 5-HT1a

Receptor v.s Functional Gradient. From this plot, we deduced it was more appropriate and representative of the data to use Spearman Correlation moving forward. Overall, these EDA scatter plots illustrate a range of patterns across modalities, from tightly constrained monotonic associations to weak correlation distributions.

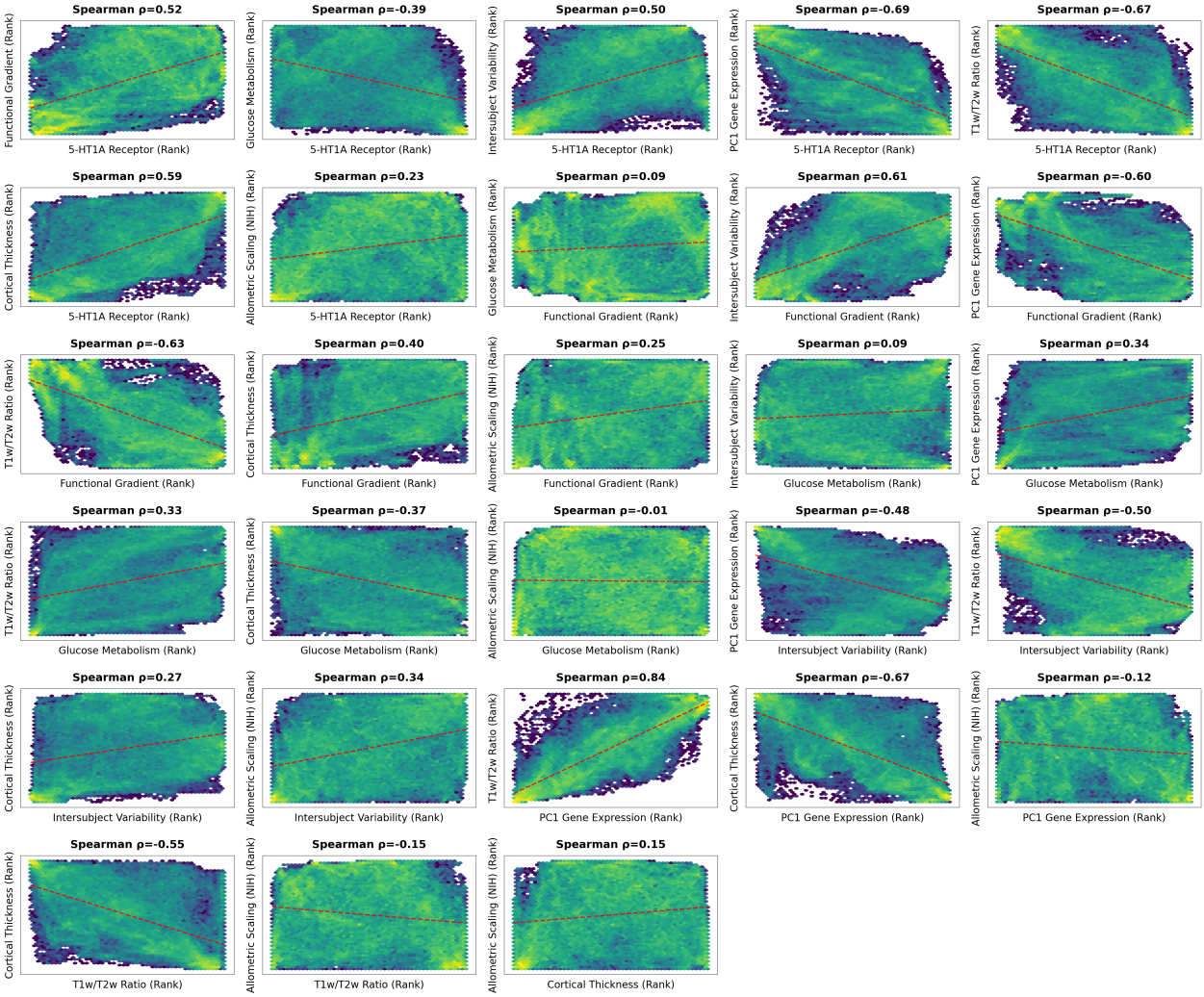

Figure 3: Ranked Pairwise Density Scatter Plots

Figure 3, illustrates the pairwise density scatter plot using ranked data instead of the raw data. Before plotting, each cortical map was converted to ranked values across regions, and pairwise relationships were assessed under the Spearman rank correlation coefficients (ρ), shown in each subplot, where the same density based binning was applied. The rank based scatter plots exhibit a range of monotonic relationships (strong positive, strong negative, and weak associations). Several subplots display a clear monotonic pattern (e.g., PC1 Gene Expression with T1w/T2w Ratio, Cortical Thickness with 5-HT1a Receptor, and Functional Gradient with Intersubject Variability). This aligns with the linear associations observed in the raw density scatter plot, but now extends to new brain map pairs. Other brain map pairs show weak monotonic association under the rank transformation, including comparisons involving Allometric Scaling NIH and Glucose Metabolism, which correspond to the

$\rho = -0.01$. Overall, the rank based scatter plots summarize the monotonic spatial relationships between cortical maps and visualize the underlying structure with the Spearman correlation.

3.1.2 Pairwise Coupling Brain Maps

Purely for visualization purposes, we created brain map images that depict the coupling rank between brain map pairs. These brain maps using a coupling score ranging from 0 (no linkage/coupling) to 1 (very strong linkage) calculated via ranking the data, creating percentiles, calculated the difference in ranks, and cubing the score to account for random noise. Below are some examples of our coupling brain maps. More brain maps can be found in Appendix A.2.1.

One issue we ran into when plotting the non-relationship coupling pairs was two brain maps with no relation exhibited high coupling or uniform bright areas on the brain map plot. Diving deeper into why this was the case, we simulated random data and performed the same coupling steps which yielded a triangle or tent distribution. This can be seen in Figure A 9 in Appendix A.2. The expected average coupling score (1—Difference) is zero, however taking into account that the data is ranked and a uniform distribution, this is false. It's instead observed that it's essentially more likely for there to be a small difference between two random points than for there to be a large difference, resulting in an average high coupling score and thus a misleading coupling brain plot. To account for this, we cubed the coupling score to better account for this phenomenon, which helped with the distribution.

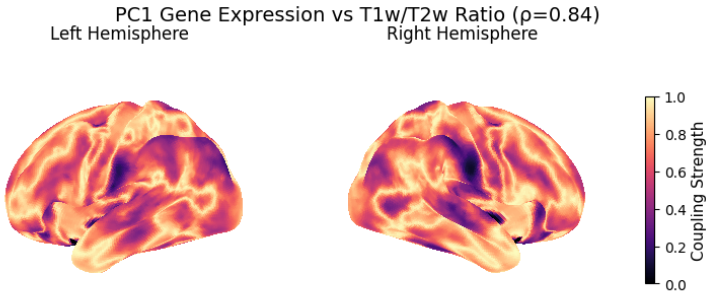

Figure 4: PC1 Gene Expression VS Myelin Ration Coupling

In Figure 4, we displayed the coupling score between PC1 Gene Expression and T1W/T2W Ratio. This is one of the linear examples from the scatter plots shown previously. For varying regions, we saw similar ranked data between the two brain maps. This brain map outlines the positive linear association between the two maps which is illustrated with the bright yellow across different regions of the cerebral cortex.

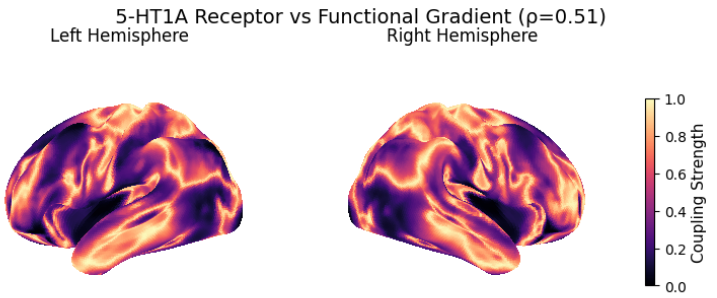

Figure 5: 5-HT1a Receptor vs Functional Gradient Coupling

Figure 5 shows the coupling score of the complex relationship between 5-HT1a Receptor and Functional Gradient. As shown in the density scatter plot, both raw data and in ranked data, we observed complex relationships such as an ”S” curve or ”hockey stick” curve, meaning high linkage in certain regions of the brain. Here, the brain map outlines the specific regions (primary sensory cortex) where there is a high coupling score compared to the low scoring regions (association cortex).

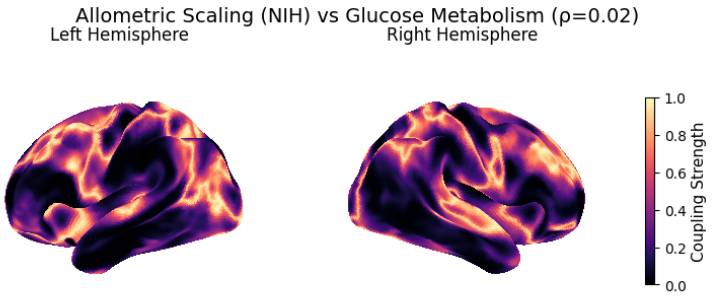

Figure 6: Allometric Scaling (NIH) vs Glucose Metabolism Coupling

Figure 6 provides an example for a coupling score brain map of a non-relationship/association between brain maps. Allometric Scaling NIH and Glucose Metabolism are not associated with a correlation coefficient of $\rho = 0.02$ such that the local rank ordering of vertices for the Allometric Scaling NIH map doesn't spatially align with the rank ordering of the Glucose Metabolism map in any specific region. The coupling brain map illustrates the low coupling score across the entire cortical surface and thus we observe more of the low, dark end of the coupling strength scale.

3.1.3 Significance Testing

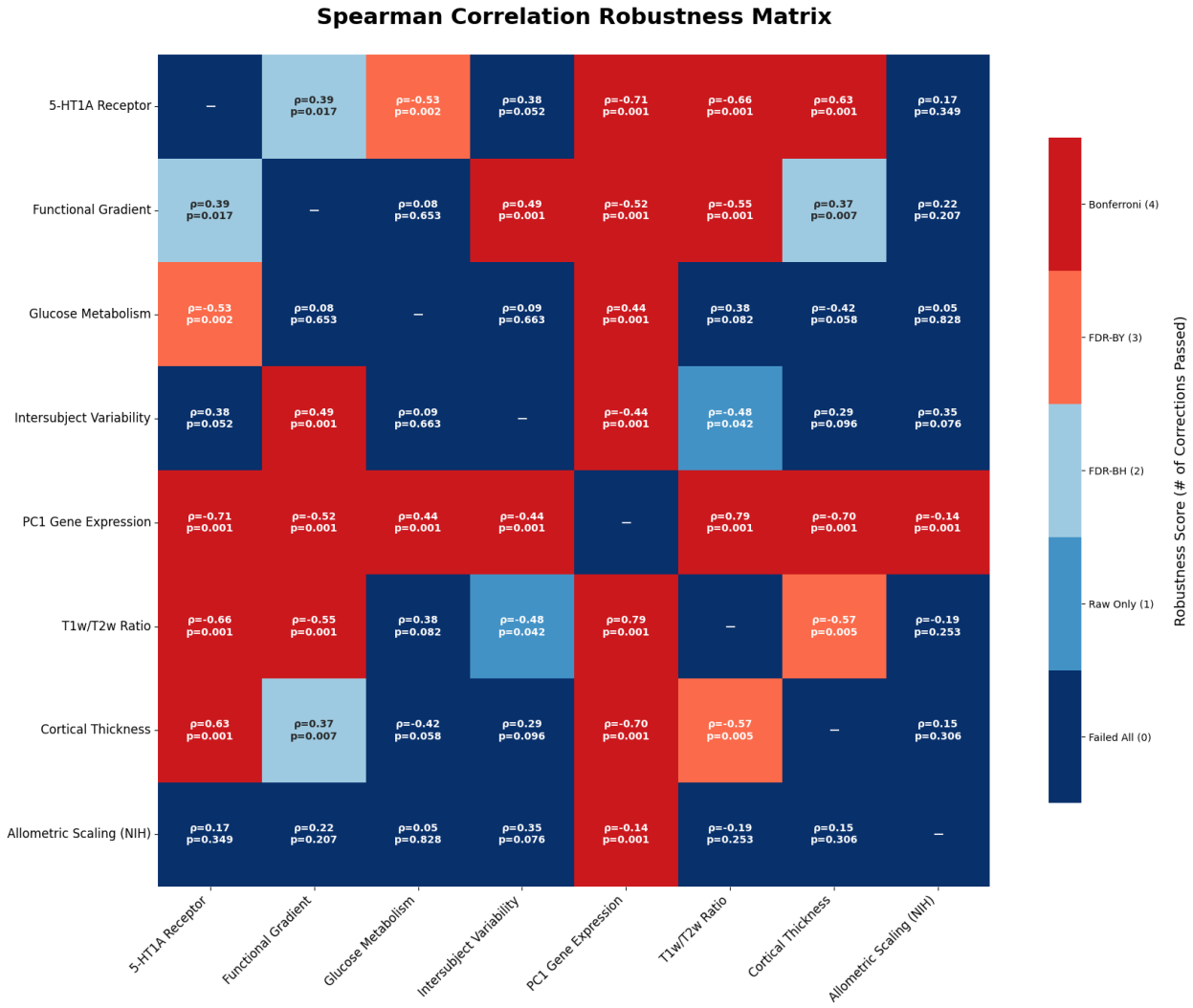

Figure 7: Multiple Test Correction Matrix

Figure 7 shows an overall summary of which brain map pairs are significant under different multiple test correction methods. In the plot, the color bar on the right acts as a robust-ness check where Bonferroni is the strictness method. A higher score (a warmer color) indicates that the correlation between two brain maps is sufficiently strong to survive more rigorous statistical corrections. This allows for an immediate visual distinction between exploratory findings (Blue) and highly robust, conservative associations (Red).

To account for the increased false positive rate associated with multiple testing, we applied three correction methods: False Discovery Rate Benjamini-Hochberg (BH) and Benjamini-Yekutieli (BY) and the Bonferroni Correction. Of the 28 unique pairs, 17 were significant uncorrected ($p < 0.05$). Notably, PC1 Gene Expression was significantly coupled with all seven other maps (T1w/T2w Ratio, Cortical Thickness, Allometric Scaling, 5-HT1a, Functional Gradient, Glucose Metabolism, and Intersubject Variability). Other significant rela-

tionships included T1w/T2w Ratio with four maps (Cortical Thickness, 5-HT1a, Functional Gradient, Intersubject Variability); Cortical Thickness with 5-HT1a and Functional Gradient; 5-HT1a with Functional Gradient and Intersubject Variability; and Intersubject Variability with Allometric Scaling and Functional Gradient. The same 17 pairs remained significant under the FDR-BH correction. However, under the Bonferroni Correction, 12 pairs retained significance: all 7 couplings with PC1 Gene Expression remained, but structural couplings were reduced to T1w/T2w Ratio with 5-HT1a and Functional Gradient; Cortical Thickness with 5-HT1a; 5-HT1a with Functional Gradient; and Intersubject Variability with Functional Gradient. The FDR-BY method identified 13 significant pairs. These included the exact same set as the Bonferroni correction, with the addition of the relationship between Cortical Thickness and T1w/T2w Ratio. As expected, no relationship was found to be significant under a correction method that was not also significant in the uncorrected analysis.

Table A 1 in Appendix A.1 summarizes the spatial null spin test results, displaying the ρ values, spin test p-values, and significance status for all 28 pairwise comparisons.

Table 1: Summary Table for Max T Correction

Map 1	Map 2	Correlation	Significant
T1w/T2W Ratio	PC1 Gene Expression	0.842	True
PC1 Gene Expression	5-HT1A Receptor	-0.690	True
T1w/T2w Ratio	5-HT1A Receptor	-0.671	True
PC1 Gene Expression	Cortical Thickness	-0.665	True
T1w/T2w Ratio	Functional Gradient	-0.629	True
Functional Gradient	Intersubject Variability	0.612	True
PC1 Gene Expression	Functional Gradient	-0.595	True
Cortical Thickness	5-HT1A Receptor	0.595	True
Functional Gradient	5-HT1A Receptor	0.519	True
T1w/T2w Ratio	Cortical Thickness	-0.553	True
PC1 Gene Expression	Allometric Scaling (NIH)	-0.117	False
T1w/T2w Ratio	Allometric Scaling (NIH)	-0.150	False
Cortical Thickness	Allometric Scaling (NIH)	0.147	False
PC1 Gene Expression	Glucose Metabolism	0.340	False
PC1 Gene Expression	Intersubject Variability	-0.477	False
T1w/T2w Ratio	Glucose Metabolism	0.333	False
T1w/T2w Ratio	Intersubject Variability	-0.499	False
Cortical Thickness	Functional Gradient	0.399	False
Cortical Thickness	Glucose Metabolism	-0.366	False
Cortical Thickness	Intersubject Variability	0.269	False
Allometric Scaling (NIH)	Functional Gradient	0.252	False
Allometric Scaling (NIH)	Glucose Metabolism	-0.013	False
Allometric Scaling (NIH)	Intersubject Variability	0.342	False
Allometric Scaling (NIH)	5-HT1A Receptor	0.225	False
Functional Gradient	Glucose Metabolism	0.092	False
Glucose Metabolism	Intersubject Variability	0.089	False
Glucose Metabolism	5-HT1A Receptor	-0.391	False
Intersubject Variability	5-HT1A Receptor	0.479	False

Table 1 summarizes the 28 brain map pairs and which are significant under the Max-T Permutation Correction method. The Max-T threshold was empirically determined to be $|\rho| > 0.511$, meaning any correlation weaker than this could have arisen by chance from random spatial overlap. We observed 10 of the 28 pairs to be significant, meaning the correlation value was greater than the largest correlation value found after running 1,000 permutation tests. This new criterion ensures that these 10 relationships represent robust biological signals that exceed the maximum background noise expected across the entire dataset, effectively controlling the Family-Wise Error Rate (FWER) at 5%.

3.2 Principal Component Analysis

PCA was performed on the 8×8 Spearman correlation matrix. The eigendecomposition yielded the following leading eigenvalues and variance explained: PC1 $\lambda_1 = 4.008$ (50.10% of total variance) and PC2 $\lambda_2 = 1.446$ (18.08%). Together, PC1 and PC2 explained 68.18% of the variance in the multimodal correlation structure. The remaining components explained 11.02% (PC3), 6.41% (PC4), 5.01% (PC5), 4.11% (PC6), 3.50% (PC7), and 1.77% (PC8).

Table 2: Eigenvalues and variance explained by each principal component.

Component	Eigenvalue	Variance explained (%)
PC1	4.008	50.10
PC2	1.446	18.08
PC3	0.882	11.02
PC4	0.513	6.41
PC5	0.401	5.01
PC6	0.329	4.11
PC7	0.280	3.50
PC8	0.142	1.77

Using loadings $\mathbf{L} = \mathbf{V}\boldsymbol{\Lambda}^{1/2}$, the PC1 and PC2 loadings (in the same map order as the correlation matrix) were calculated. These loadings are visualized in the PCA heatmap and PC1–PC2 loading scatter.

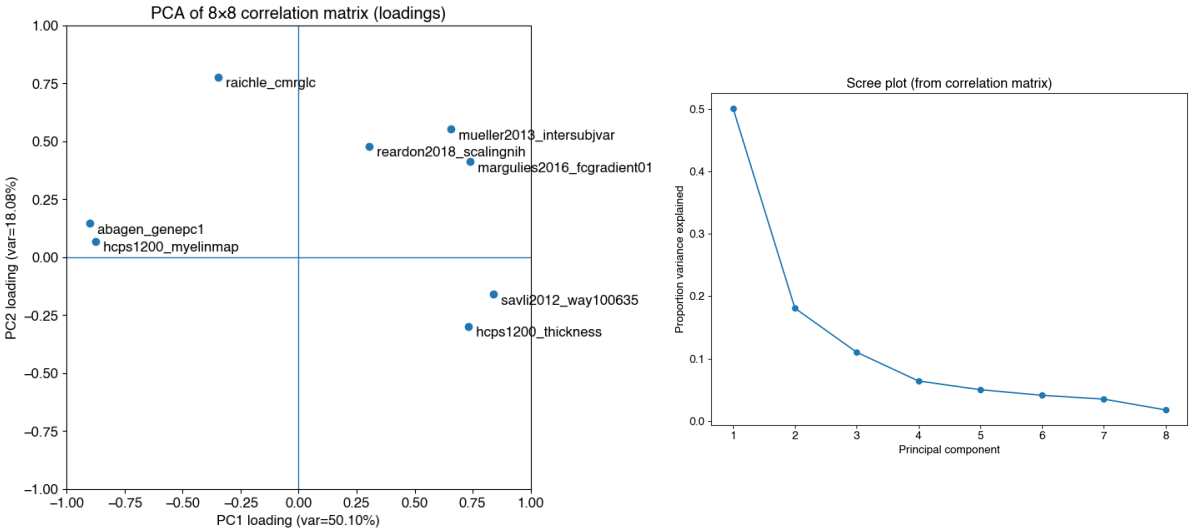

Figure 8: PC 1 Loading vs. PC 2 Loading Scatter Plot and Scree Plot of Proportion of Variance Explained by Each PC

3.3 Subgroup Connectivity Analysis

Hierarchical clustering

Hierarchical clustering was applied to the Spearman correlation matrix using the distance transform $\mathbf{D} = \mathbf{1} - \mathbf{R}$ with average linkage. Cutting the dendrogram into $k = 2$ clusters

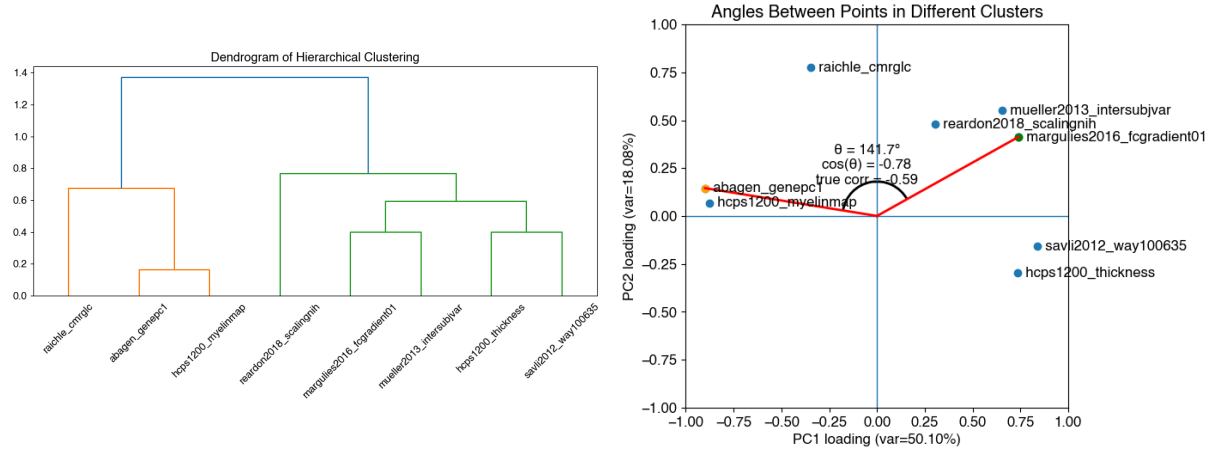

Figure 9: Dendrogram of hierarchical clustering with $k = 2$ clusters and angles in PC 1 vs. PC 2 loadings between two points in opposite groups

(`criterion="maxclust"`) produced the following assignments:

Table 3: Two-cluster solution from hierarchical clustering (average linkage) on correlation-derived distances $\mathbf{D} = \mathbf{1} - \mathbf{R}$.

Map Description/Source	Brain map	Cluster
abagen_genepc1	PC1 Gene Expression	1
hcps1200_myelinmap	T1W/T2W Ratio	1
raichle_cmrglc	Glucose Metabolism	1
hcps1200_thickness	Cortical Thickness	2
reardon2019_scalingnih	Allometric Scaling NIH	2
savli2012_way100635	5-HT1a Receptor	2
margulies2016_fcgradient01	Functional Gradient	2
mueller2013_intersubvar	Intersubject Variability	2

Within- and between-cluster connectivity. Subgroup connectivity was summarized by mean Spearman correlation within each cluster (off-diagonal entries only) and mean correlation between clusters. The within-cluster means were $\bar{r}_{\text{within},1} = 0.497$ for Cluster 1 and $\bar{r}_{\text{within},2} = 0.378$ for Cluster 2. The between-cluster mean correlation (averaged over all cross-cluster pairs) was $\bar{r}_{\text{between}} = -0.370$.

Table 4: Subgroup connectivity summary (mean Spearman correlations). Within-cluster means exclude diagonal entries; between-cluster mean averages all cross-cluster pairs.

Connectivity summary	**Mean correlation**
Within Cluster 1 ($\bar{r}_{\text{within},1}$)	0.497
Within Cluster 2 ($\bar{r}_{\text{within},2}$)	0.378
Between clusters ($\bar{r}_{\text{between}}$)	-0.370

4 Discussion

4.1 Multimodal Correlation

Our comprehensive exploratory data analysis (EDA) and significance testing set a robust foundation for our Principal Component Analysis and Subgroup Analysis. Ranging from our multimodal correlation matrix to our significance testing and multiple test correction methods, we saw how non-uniform the human cortex is. Initially, the pairwise density scatter plots showed many relationships are highly complex, depicting an 'S' or 'hockey stick' curve, meaning the structural and chemical modalities are not globally linked, but rather they are tightly coupled in primary sensory regions and highly uncoupled in the association cortex. We saw this in Figure 5 5-HT1a v.s Functional Gradient Coupling brain map. In addition to this, our significance and multiple test testing addresses the spatial autocorrelation issues inherent in neuroimaging data and the inflated false positive rate after running 28 correlation tests. From the FDR-BH, FDR-BY, and Bonferroni method, we saw very little change of significance across all three methods, indicating that the final significant correlations are very strong biological signals. Furthermore, the Max-T Permutation testing yielded 10 of 28 pairs significant under the $|\rho| > 0.511$ threshold. From these results, we can conclude that these 10 relationships represent true fundamental structural and chemical linkages, proving they are not merely artifacts of the brain's inherent geometric smoothness. Compared to previous work, our EDA findings support the tethering hypothesis from "The Organization of The Human Cerebellum Estimated by Intrinsic Functional Connectivity" (Buckner et al. 2011). Buckner et al. hypothesized that the sensory and motor regions are evolutionarily tethered to molecular and structural gradients and the association cortex (expanding more rapidly than sensory/motor regions), is untethered to allow for higher order cognition such as abstract reasoning, complex decision making, and social cognition. Our EDA visually supports this claim, specifically our ranked density scatter plots and coupling brain maps show this relationship in certain regions. Our primary impact is to implement a robust and reproducible analytical pipeline that can be used in the neuroscience community. By combining our EDA and statistical framework, we aim to use our pipeline to further explore the tethered relationship between the structural and chemical modalities.

4.2 Principal Component Analysis

The Principal Component Analysis revealed a highly compressed low-dimensional structure in the brain's multimodal organization. PC1, explaining 50.10% of the variance, functions as a global "coupling axis" that captures shared spatial variation across nearly all modalities. In contrast, PC2 (18.08%) serves as a "segregation axis," primarily differentiating between the structural maps (loading on one end) and neurochemical/functional gradients (loading on the other).

The scree plot indicates that these two components account for nearly 70% of the total multimodal covariance, suggesting that the brain's complex landscape can be reduced to a few dominant organizational principle's. The orthogonality of PC1 and PC2 supports the idea that while there is a general global pattern of cortical organization, there exists a secondary, independent dimension where structural features (like cortical thickness) and functional/chemical features (like 5-HT1a receptor density) diverge.

Additionally, our PCA results echo the macroscale gradients identified by Margulies et al. (2016), reinforcing the idea that the brain is organized along a principal axis that transitions from unimodal sensory regions to transmodal default-mode regions.

4.3 Subgroup Analysis

The subgroup connectivity analysis and hierarchical clustering results statistically confirm our initial hypothesis of partially segregated modes. The dendrogram naturally partitioned the maps into two clusters that largely correspond to "Inward-oriented/Structural" (Cluster 1) and "Outward-oriented/Functional" (Cluster 2) systems.Quantitatively, the strength of coupling within these clusters ($\bar{r}_{within,1} = 0.497$ and $\bar{r}_{within,2} = 0.378$) significantly exceeded the absolute mean correlation between clusters ($\bar{r}_{between} = -0.370$). This indicates that brain maps within the same biological layer are more spatially correlated with one another than they are with maps in the opposing group. The negative between-group mean correlation further highlights a inverse relationship between certain structural and functional markers, providing evidence for a structural and functional decoupling in specific cortical zones.

4.4 Impact and Applicability

A primary contribution of this work is the establishment of a robust, reproducible, and statistically rigorous analytical pipeline for multimodal neuroimaging integration. By standardizing diverse imaging modalities (PET, fMRI, sMRI) into a unified coordinate framework and applying stringent spatial null models, this study provides a normative baseline for cortical covariance. This methodological framework holds significant translational potential; it can be adapted to investigate the degradation of structural-functional coupling in neurodegenerative pathologies or psychiatric conditions, where normative macroscale gradients are frequently disrupted.

4.5 Limitations and Future Work

Despite the statistical robustness of these findings, several methodological limitations must be acknowledged. The reliance on PCA, inherently a linear dimensionality reduction technique, may obscure complex, higher-order non-linear interactions between modalities, even with the application of rank-transformed data. Additionally, the present analysis is constrained to an eight-map ensemble.

Future investigations should incorporate a broader array of neurochemical targets such as dopaminergic or GABAergic receptor densities and high-resolution transcriptomic data to yield a more comprehensive characterization of cortical organization. Subsequent research could also extend this pipeline to longitudinal cohorts, enabling the characterization of multimodal coupling trajectories across neurodevelopment and aging, or explore how individual variance in spatial tethering correlates with specific cognitive phenotypes and behavioral traits.

5 Conclusion

Our project aimed to create and implement an anayltical pipeline to examine the relationship between the structural/physical and chemical/functional layers of the brain. Using 8 brain maps (4 structural, 4 chemical) from the neuromaps' toolbox (Markello et al. 2022), as well as the Alexander Bloch Spin Test (Alexander-Bloch et al. 2018), we tested our hypothesis about the cortical organization and began our testing under the theory that these two layers in the brain work as independent modes. Based on our preliminary findings, we saw strong associations between PC1 Gene Expression, T1W/T2W Ratio (Myelin), Cortical Thickness, 5-HT1a Receptor, and Functional Gradient. Given the very complex relationships between brain maps, we opted to use Spearman Rank Correlation ρ, a non-linear correlation method. We observed many relationships to be monotonic but not strictly linear indicating regional linkage. During this process, we implemented multiple tests correction methods to account for the inflated false positives during correlation testing. Specifically, after running the max-T Permutation correction, we saw 10 relationships still significant, meaning these 10 pairs were persisted under the strict family wise error threshold, demonstrating that these correlations aren't due to spurious spatial overlap or chance. From running PCA, we saw about 68% of the variance explained by the first two principal components: PC1 (acting as a global coupling axis) and PC2 (showing differentiated structural and neurochemical maps). This complex hierarchy of brain layers can be displayed in a low dimensional organization, meaning our correlation matrix isn't random and we can summarize majority of the variance with a few principal components. Following with Subgroup (Hierarchical clustering) Analysis with our multimodal correlation matrix, we saw two clusters form: Cluster #1 containing PC1 Gene Expression, T1w/T2w Ratio (Myelin), Glucose Metabolism, and Cluster #2 containing Cortical Thickness, Allometric Scaling (NIH), 5-HT1A Receptor, Functional Gradient, Intersubject Variability. Given these two clusters, we saw the within-cluster mean correlation greater than the between-cluster mean correlation, supporting the complex relationships inherent to the brain and the partial segregation

rather than complete independent modes. Based on our findings, we conclude that the cortex exhibits structured multimodal covariance, with structural and functional gradients systematically aligned across specific regions. This organization isn't random and reflects partial segregation and interacting modes, rather than fully independent modes. All together, these patterns suggest that the large scale cortical layout is defined by coordinated integration across modalities.

References

Alexander-Bloch, A., H. Shou, S. Liu, T. D. Satterthwaite, D. C. Glahn, R. T. Shinohara, S. N. Vandekar, and A. Raznahan. 2018. "On testing for spatial correspondence between maps of human brain structure and function." *NeuroImage* 178: 540–551. [Link]

Benjamini, Y., and Y. Hochberg. 1995. "Controlling the false discovery rate: a practical and powerful approach to multiple testing." *Journal of the Royal Statistical Society: Series B (Methodological)* 57(1): 289–300

Buckner, Randy L, Fenna M Krienen, Angela Castellanos, Julio C Diaz, and BT Thomas Yeo. 2011. "The organization of the human cerebellum estimated by intrinsic functional connectivity." *Journal of neurophysiology* 106(5): 2322–2345

Burt, Joshua B, Murat Demirtaş, William J Eckner, Natasha M Navejar, Jie Lisa Ji, William J Martin, Alberto Bernacchia, Alan Anticevic, and John D Murray. 2018. "Hierarchy of transcriptomic specialization across human cortex captured by structural neuroimaging topography." *Nature neuroscience* 21(9): 1251–1259

Glasser, M. F., S. M. Smith, D. S. Marcus, J. L. R. Andersson, E. J. Auerbach, T. E. J. Behrens, T. S. Coalson, M. P. Harms, M. Jenkinson, S. Moeller, and D. C. Van Essen. 2016. "The Human Connectome Project's neuroimaging approach." *Nature* 536: 171–178. [Link]

Hunter, J. D. 2007. "Matplotlib: A 2D graphics environment." *Computing in Science & Engineering* 9(3): 90–95. [Link]

Jolliffe, I. T. 2002. *Principal Component Analysis*. Springer

Margulies, D. S., J. Böttger, A. Watanabe, and J. Smallwood. 2016. "Situating the default-mode network along a principal gradient of macroscale cortical organization." *Proceedings of the National Academy of Sciences* 113(44): 12574–12579. [Link]

Markello, R. D., A. Arnatkeviciute, J.-B. Poline, and B. Mišić. 2021. "Standardizing workflows in imaging transcriptomics with the abagen toolbox." *eLife* 10, p. e72129. [Link]

Markello, R. D., J. Y. Hansen, Z.-Q. Liu, V. Bazinet, G. Shafiei, L. E. Suarez, N. Blostein, J. Seidlitz, S. Baillet, T. D. Satterthwaite, M. M. Chakravarty, A. Raznahan, and B. Mišić. 2022. "neuromaps: structural and functional interpretation of brain maps." *Nature Methods* 19: 1472–1479. [Link]

Markello, R., J. Hansen, Z.-Q. Liu, V. Bazinet, G. Shafiei, L. Suarez, and B. Mišić. 2024. "neuromaps: structural and functional interpretation of brain maps (version 0.0.5)." Zen-

odo. [Link]

Mueller, S., D. Wang, M. D. Fox, B. T. Yeo, J. Sepulcre, M. R. Sabuncu, R. Shafee, J. Lu, and H. Liu. 2013. "Individual variability in functional connectivity architecture of the human brain." *Neuron* 77 (3): 586–595. [Link]

Oakes, T.R., T. Johnstone, K.S. Ores Walsh, L.L. Greischar, A.L. Alexander, A.S. Fox, and R.J. Davidson. 2005. "Comparison of fMRI motion correction software tools." *NeuroImage* 28 (3): 529–543. [Link]

Reardon, P. K., J. Seidlitz, S. N. Vandekar, S. Liu, R. Patel, M. T. M. Park, A. Alexander-Bloch, L. S. Clasen, J. D. Blumenthal, F. Lalonde et al. 2018. "Normative brain size variation and brain shape diversity in humans." *Science* 360 (6394): 1222–1227. [Link]

Robinson, E. C., K. Garcia, M. F. Glasser, Z. Chen, T. Coalson, A. Makropoulos, J. Bozek, R. Wright, A. Schuh, M. Webster et al. 2018. "Multimodal surface matching with higher-order smoothness constraints." *NeuroImage* 167: 453–465. [Link]

Robinson, E. C., S. Jbabdi, M. F. Glasser, J. Andersson, G. C. Burgess, M. P. Harms, S. M. Smith, D. C. Van Essen, and M. Jenkinson. 2014. "MSM: a new flexible framework for multimodal surface matching." *NeuroImage* 100: 414–426. [Link]

Savli, Markus, Andreas Bauer, Markus Mitterhauser, Yu-Shin Ding, Andreas Hahn, Tina Kroll, Alexander Neumeister, Daniela Haeusler, Johanna Ungersboeck, Shannan Henry et al. 2012. "Normative database of the serotonergic system in healthy subjects using multi-tracer PET." *Neuroimage* 63 (1): 447–459

Sedgwick, Philip. 2012. "Multiple significance tests: the Bonferroni correction." *Bmj* 344

Vaishnavi, S. N., A. G. Vlassenko, M. M. Rundle, A. Z. Snyder, M. A. Mintun, and M. E. Raichle. 2010. "Regional aerobic glycolysis in the human brain." *Proceedings of the National Academy of Sciences* 107 (41): 17757–17762. [Link]

Virtanen, Pauli, Ralf Gommers, Travis E. Oliphant, Matt Haberland, Tyler Reddy, David Cournapeau, Evgeni Burovski, Pearu Peterson, Warren Weckesser, Jonathan Bright, Stéfan J. van der Walt, Matthew Brett, Joshua Wilson, K. Jarrod Millman, Nikolay Mayorov, Andrew R. J. Nelson, Eric Jones, Robert Kern, Eric Larson, C J Carey, İlhan Polat, Yu Feng, Eric W. Moore, Jake VanderPlas, Denis Laxalde, Josef Perktold, Robert Cimrman, Ian Henriksen, E. A. Quintero, Charles R. Harris, Anne M. Archibald, Antônio H. Ribeiro, Fabian Pedregosa, Paul van Mulbregt, and SciPy 1.0 Contributors. 2020. "SciPy 1.0: Fundamental Algorithms for Scientific Computing in Python." *Nature Methods* 17: 261–272. [Link]

White, Tonya, Jan van der Ende, and Thomas E Nichols. 2019. "Beyond Bonferroni revisited: concerns over inflated false positive research findings in the fields of conservation genetics, biology, and medicine." *Conservation Genetics* 20 (4): 927–937

Wu, Jianxiao, Gia H Ngo, Douglas Greve, Jingwei Li, Tong He, Bruce Fischl, Simon B Eickhoff, and BT Thomas Yeo. 2018. "Accurate nonlinear mapping between MNI volumetric and FreeSurfer surface coordinate systems." *Human brain mapping* 39 (9): 3793–3808

Appendices

A.1 Additional Tables

Table A 1: Multiple Test Comparisons Table

	Map 1	Map 2	Spearman	P-val (Uncorrected)	Significant (Uncorrected)	Significant (Bonf)	Significant (FDR-BH)	Significant (FDR-BY)
0	T1w/T2w Ratio	PC1 Gene Expression	0.842	0.001	True	True	True	True
1	Cortical Thickness	PC1 Gene Expression	-0.665	0.001	True	True	True	True
2	Cortical Thickness	T1w/T2w Ratio	-0.553	0.002	True	False	True	True
3	Allometric Scaling (NIH)	PC1 Gene Expression	-0.117	0.001	True	True	True	True
4	Allometric Scaling (NIH)	T1w/T2w Ratio	-0.150	0.467	False	False	False	False
5	Allometric Scaling (NIH)	Cortical Thickness	0.147	0.373	False	False	False	False
6	5-HT1A Receptor	PC1 Gene Expression	-0.690	0.001	True	True	True	True
7	5-HT1A Receptor	T1w/T2w Ratio	-0.671	0.001	True	True	True	True
8	5-HT1A Receptor	Cortical Thickness	0.595	0.001	True	True	True	True
9	5-HT1A Receptor	Allometric Scaling (NIH)	0.225	0.194	False	False	False	False
10	Functional Gradient	PC1 Gene Expression	-0.595	0.001	True	True	True	True
11	Functional Gradient	T1w/T2w Ratio	-0.629	0.001	True	True	True	True
12	Functional Gradient	Cortical Thickness	0.399	0.016	True	False	True	False
13	Functional Gradient	Allometric Scaling (NIH)	0.252	0.100	False	False	False	False
14	Functional Gradient	5-HT1A Receptor	0.519	0.001	True	True	True	True
15	Glucose Metabolism	PC1 Gene Expression	0.340	0.001	True	True	True	True
16	Glucose Metabolism	T1w/T2w Ratio	0.333	0.119	False	False	False	False
17	Glucose Metabolism	Cortical Thickness	-0.366	0.054	False	False	False	False
18	Glucose Metabolism	Allometric Scaling (NIH)	-0.013	0.927	False	False	False	False
19	Glucose Metabolism	5-HT1A Receptor	-0.391	0.061	False	False	False	False
20	Glucose Metabolism	Functional Gradient	0.092	0.613	False	False	False	False
21	Intersubject Variability	PC1 Gene Expression	-0.477	0.001	True	True	True	True
22	Intersubject Variability	T1w/T2w Ratio	-0.499	0.007	True	False	True	False
23	Intersubject Variability	Cortical Thickness	0.269	0.124	False	False	False	False
24	Intersubject Variability	Allometric Scaling (NIH)	0.342	0.028	True	False	True	False
25	Intersubject Variability	5-HT1A Receptor	0.497	0.009	True	False	True	False
26	Intersubject Variability	Functional Gradient	0.612	0.001	True	True	True	True
27	Intersubject Variability	Glucose Metabolism	0.089	0.669	False	False	False	False

A.2 Additional Figures

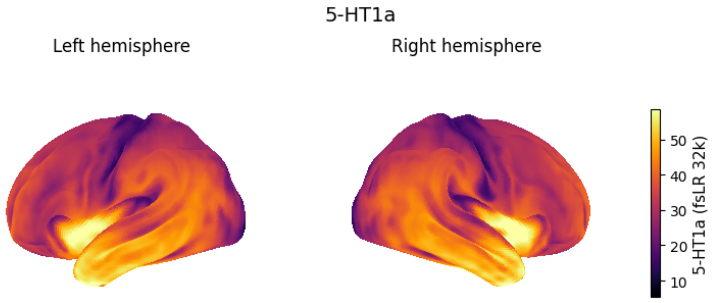

Figure A 1: 5-HT1a Receptor

The 5-HT1a brain map shows the density of the 5-HT1a receptor, otherwise known as the Serotonin 1A Receptor. Serotonin is the neurotransmitter that regulates mood, anxiety, and stress (also known as the "happy chemical"). The 5-HT1a is a type of protein that sits on the surface of neurons across the brain and receives the serotonin neurotransmitters. When the 5-HT1a receptors and serotonin meet, it tells the neurons in that region to stop firing or to "slow down". In the brain map, the lighter colored regions are areas of the brain that are highly dense with these 5-HT1a receptors. These lighter colored areas are seen at the emotional centers of the brain (The Limbic System) in the temporal lobe. It's important to have these high density areas of the receptor to essentially manage human emotions and to calm the signals neurons are sending. The darker colored regions represent less dense areas of the brain meaning there are less receptors. These regions are found in the motor strip (top of the brain) as well as the visual cortex (back of the brain) which are known for fast sensory processing. This includes touch, sight, and motor commands.

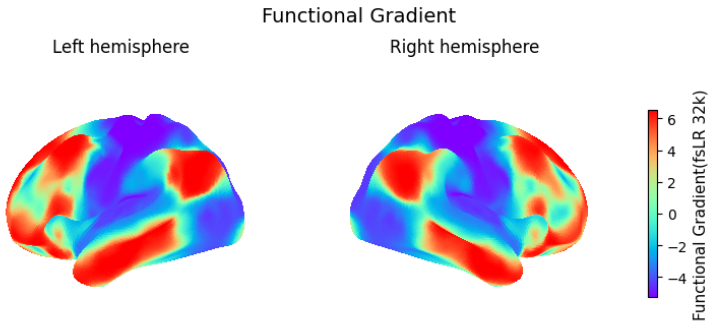

Figure A 2: Functional Gradient

The Functional Gradient brain map defines the brain's primary hierarchy of information flow (how different regions communicate with each other), organizing the cortex from sensory

processing (unimodal) to abstract cognition (transmodal). Unimodal regions (low gradient values, purple areas) process raw sensory data and accounts for motor functionality, while transmodal regions (high gradient values, red regions) are responsible for complex thought far removed from immediate sensory input such as abstract thought and self referential processing. By comparing this functional hierarchy to our structural maps, we can see whether the ”traffic pattern” in sensory regions is strictly constrained by the physical components and whether this constraint dissolves in transmodal areas.

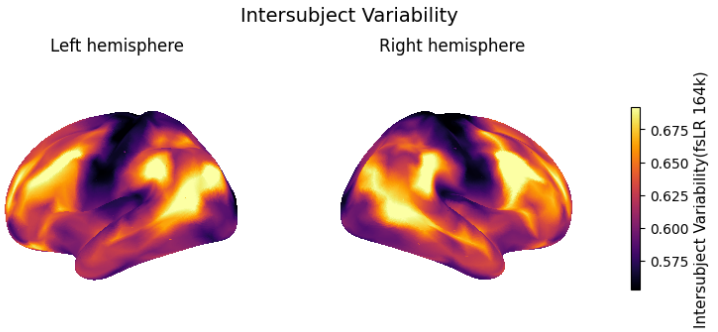

Figure A 3: Intersubject Variability

The Intersubject Variability brain map quantifies how functional brain organization differs across individuals. The functional connectivity represents how each region works together to perform function such as memory or attention. Lighter regions (transmodal regions) of the brain represent a big variability in brains maps. The brain activity patterns differ a lot person to person, such as personality, and show individually more ”custom” cognitive networks. Darker regions (unimodal regions) of the brain represent a smaller variability between brains. This can be thought of as ’factory settings’ or ’hard wired’ infastructure of the brain. For example, the visual cortex, how people see colors and light, is generally similar among people. We can see that the sensory regions are more consistent among individuals while high order cognitive function regions very more.

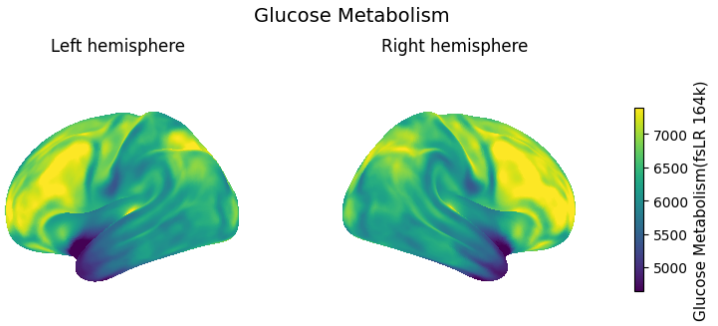

Figure A 4: Glucose Metabolism

The Glucose Metabolism brain map tracks how much glucose each brain region uses as its

primary energy source. This map reflects the energetic cost of maintaining spontaneous neural activity and synaptic signaling. Unimodal sensory regions (darker areas, dark blue) represent low glucose usage meaning there is efficient stimulus-driven activity seen in areas like the as visual and somatosensory cortex. Transmodal regions (lighter areas, yellow) show significantly higher metabolic demands, which is common in regions supporting flexible cognition, memory, and self-referential processing.

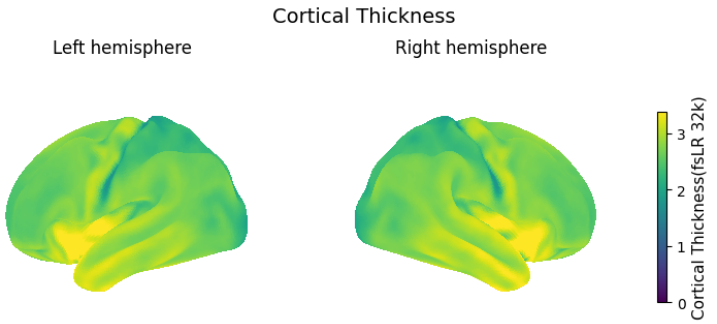

Figure A 5: Cortical Thickness

The Cortical Thickness brain map measures the physical depth of the gray matter ribbon, representing the distance between the white matter surface and the pial surface. In the context of cortical hierarchy, this map often displays an inverse relationship with myelination. The darker regions (low thickness) generally correspond to primary sensory and motor areas, such as the visual cortex and the central sulcus. These areas are structurally dense and heavily myelinated but physically thinner. Conversely, the lighter regions (high thickness) are found in the transmodal association cortex, including the temporal pole and prefrontal cortex. These thicker regions support complex, integrative processing and are less constrained by immediate sensory inputs.

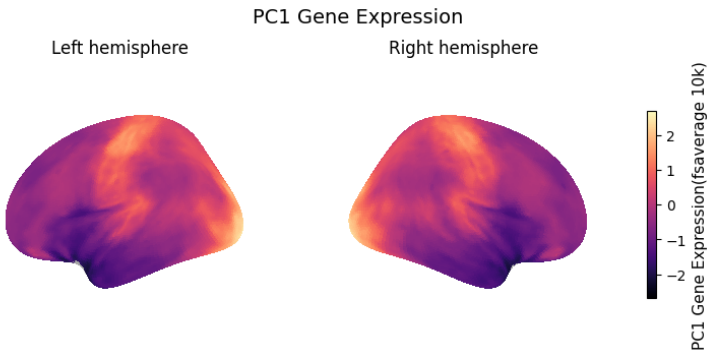

Figure A 6: PC1 Gene Expression

The PC1 Gene Expression brain map represents the first principal component of transcriptional activity across the human brain, derived from the Allen Human Brain Atlas. This map

captures the dominant axis of genetic organization, accounting for the largest variance in gene expression profiles. It effectively illustrates a molecular hierarchy that underpins the brain's structural and functional gradients. Lighter regions indicate areas with gene expression profiles characteristic of sensorimotor processing (strongly correlated with high myelination), while darker regions reflect genetic profiles associated with synaptic plasticity and higher-order cognitive functions found in the association cortex. This genetic patterning provides the molecular blueprint for the macroscopic gradients observed in other maps.

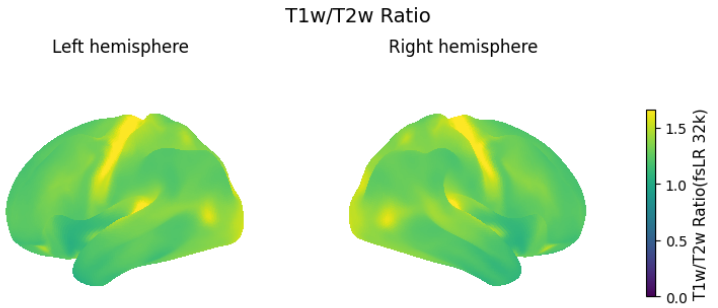

Figure A 7: T1W/T2W Ratio (Meylin)

The T1W/T2W Ratio brain map serves as a non-invasive neuroimaging proxy for intracortical myelin content. Myelin acts as an insulator for axons, allowing for rapid signal transmission essential for processing sensory inputs and motor commands. Consequently, the lighter regions (high ratio) represent heavily myelinated areas, such as the primary motor and visual cortices, which function like high-speed highways for neural data. The darker regions (low ratio) correspond to lightly myelinated association areas. These regions have less structural rigidity, allowing for greater synaptic plasticity and slower, more integrative processing required for abstract thought and decision-making.

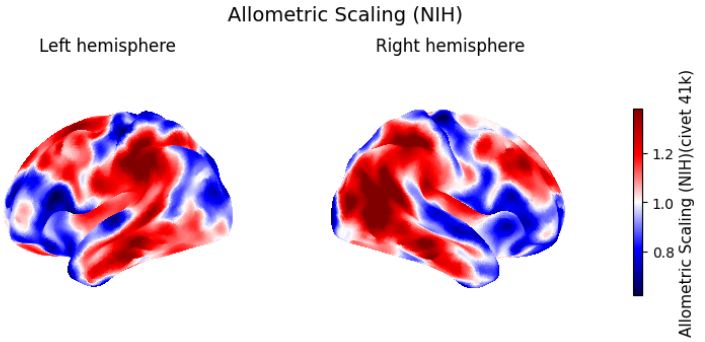

Figure A 8: Allometric Scaling NIH

The Allometric Scaling (NIH) brain map depicts how the size of specific brain regions scales relative to the total brain size across individuals. This map captures the non-linear expan-

sion of cortical surface area. Lighter regions represent areas with positive allometric scaling, meaning they expand disproportionately as total brain size increases. These are typically evolutionarily recent association networks involved in complex cognition. Darker regions represent areas with negative or hypo-metric scaling, which remain relatively stable in size regardless of total brain dimensions. These generally correspond to phylogenetically older, conserved systems such as the limbic and sensorimotor regions, representing the biological 'core' distinct from the highly variable expansion of cognitive areas.

In Figure A 9, we displayed the triangle (or tent) distribution of the random ranked uniform data to simulate the effects of the expected coupling score (1—Difference between points). We saw how the average absolute difference between two points was 0.33, and thus a coupling score of 0.66. To combat the high floor noise of the non-related brain map pairs, we cubed the coupling scores prior to plotting. As seen on the right subplot, the distribution starts to shift to the left, 'flatten' the distribution, and bring the average coupling score to 0.40.

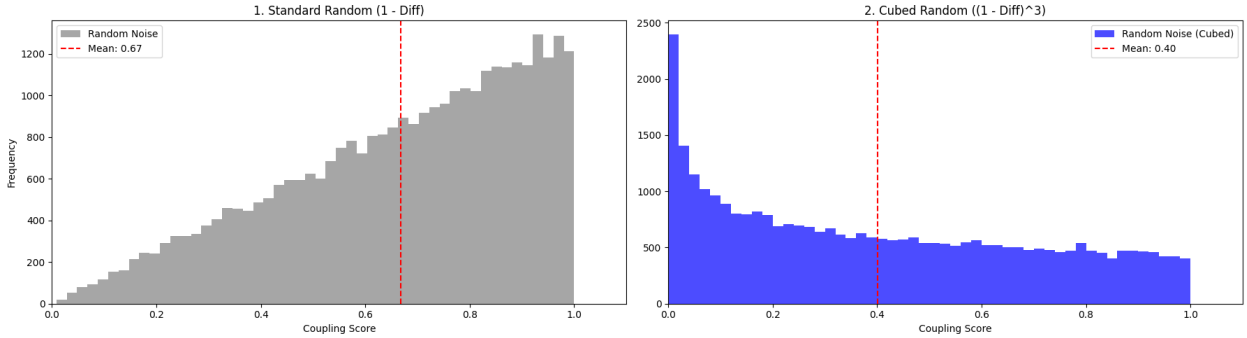

Figure A 9: Random Permutation for Coupling Score

In Figure A 10, we plotted the full multimodal correlation matrix using the Pearson r Correlation coefficient. This was used to compare against the correlation matrix using the Spearman ρ Correlation coefficient in Figure 1. It's important to note Pearson r was not used for our analysis as our findings would be misleading. We displayed the same brain map pairs and color scheme to show the positive and negative correlations.

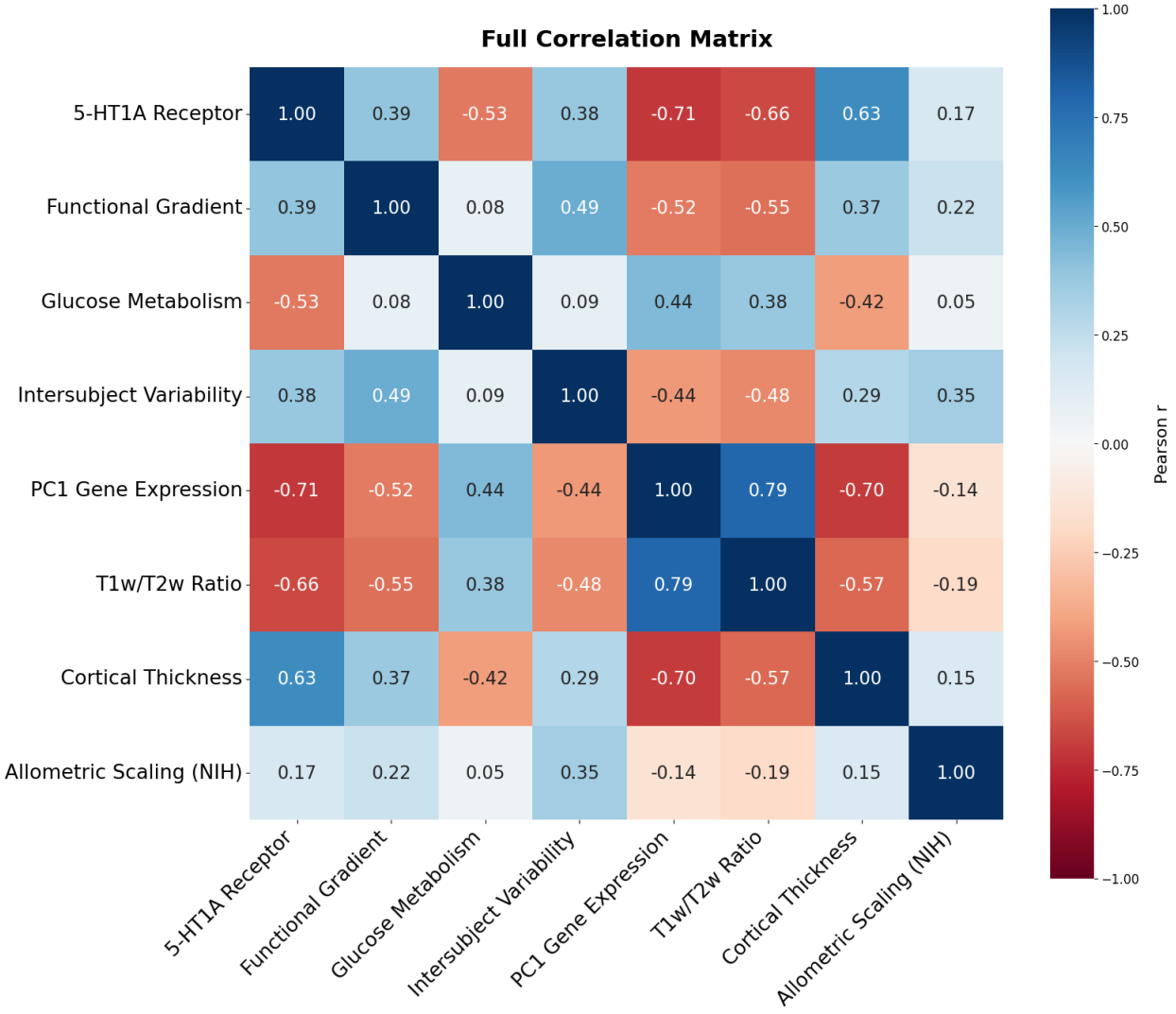

Figure A 10: Multimodal Correlation Matrix with Pearson Correlation Coefficient

A.2.1 Coupling Brain Maps

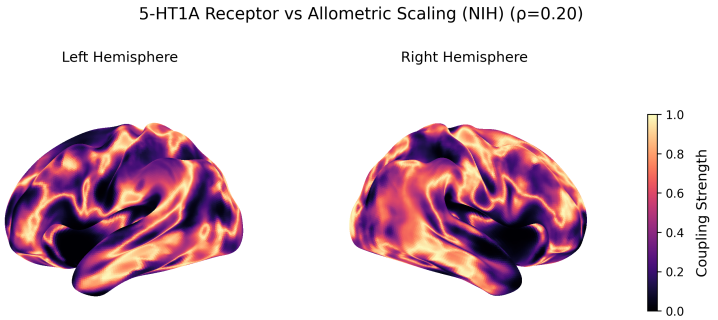

Figure A 11: 5-HT1A Receptor v.s Allometric Scaling (NIH) Coupling Brain Map

Figure A 11 shows the coupling score of the weak positive relationship between 5-HT1a Receptor and Allometric Scaling (NIH) with $\rho = 0.20$. The spatial patterns between the two brain maps are generally independent.

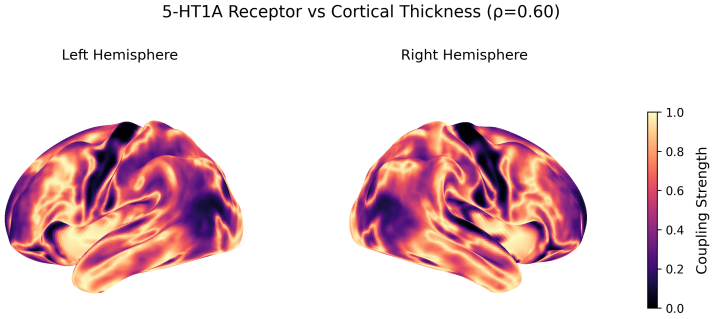

Figure A 12: 5-HT1A Receptor v.s Cortical Thickness Coupling Brain Map

Figure A 12 shows the coupling score of the strong positive relationship between 5-HT1a Receptor and Cortical Thickness with $\rho = 0.60$. The high values of both maps corerpsond to the same vertices and are tethered together.

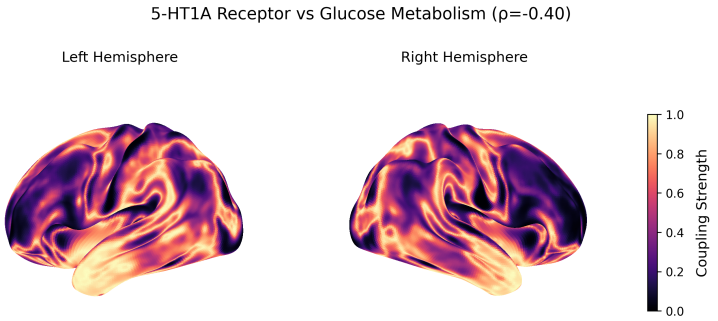

Figure A 13: 5-HT1A Receptor v.s Glucose Metabolism Coupling Brain Map

Figure A 13 shows the coupling score of the moderate negative relationship between 5-HT1a Receptor and Glucose Metabolism with ρ = -0.40. The brain maps are inversely related, demonstrating a general global trend.

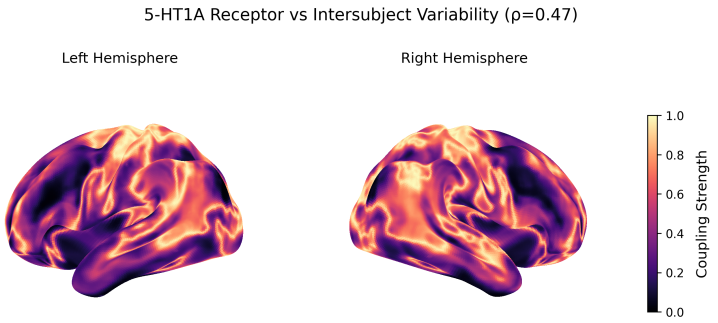

Figure A 14: 5-HT1A Receptor v.s Intersubject Variability Coupling Brain Map

Figure A 14 shows the coupling score of the moderate positive relationship between 5-HT1a Receptor and Intersubject Variability with $\rho = 0.47$. The brain maps are generally tethered globally.

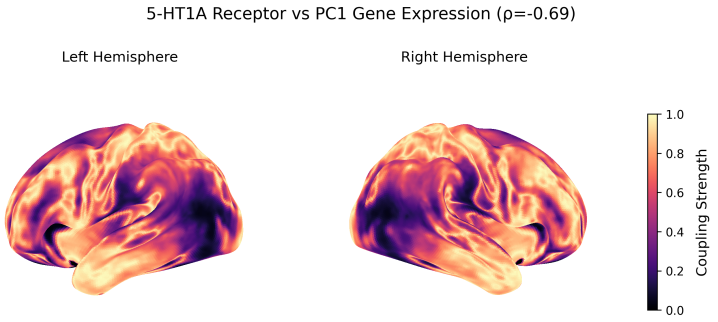

Figure A 15: 5-HT1A Receptor v.s PC1 Gene Expression Coupling Brain Map

Figure A 15 shows the coupling score of the strong negative relationship between 5-HT1a Receptor and PC1 Gene Expression with ρ = -0.69. The brain maps are mutually exclusive and are inversely tethered.

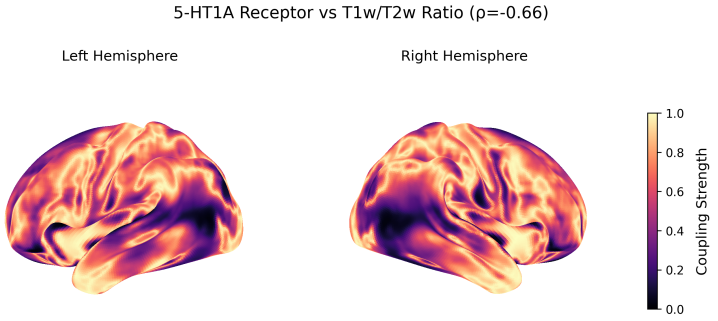

Figure A 16: 5-HT1A Receptor v.s T1W/T2W Ratio Coupling Brain Map

Figure A 16 shows the coupling score of the strong negative relationship between 5-HT1a Receptor and T1W/T2W Ratio with ρ = -0.66. The brain maps are mutually exclusive and are inversely tethered.

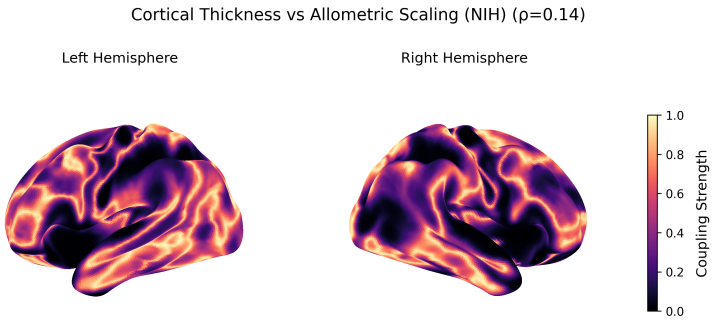

Figure A 17: Cortical Thickness v.s Allometric Scaling (NIH) Coupling Brain Map

Figure A 17 shows the coupling score of the weak positive relationship between Allometric Scaling (NIH) and Cortical Thickness with ρ = 0.14. The brain maps have no spatial patterns related to each other.

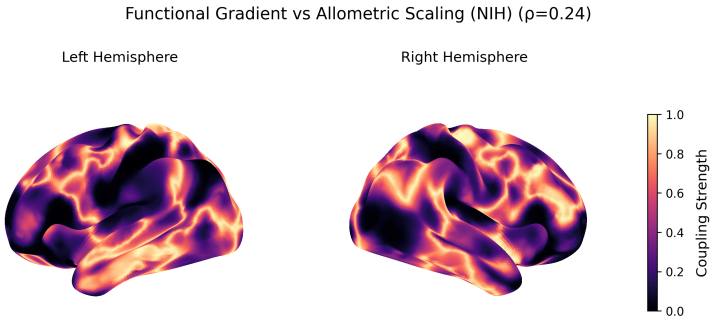

Figure A 18: Functional Gradient v.s Allometric Scaling (NIH) Coupling Brain Map

Figure A 18 shows the coupling score of the weak positive relationship between Allometric Scaling (NIH) and Functional Gradient with ρ = 0.24. The brain maps have no spatial patterns related to each other.

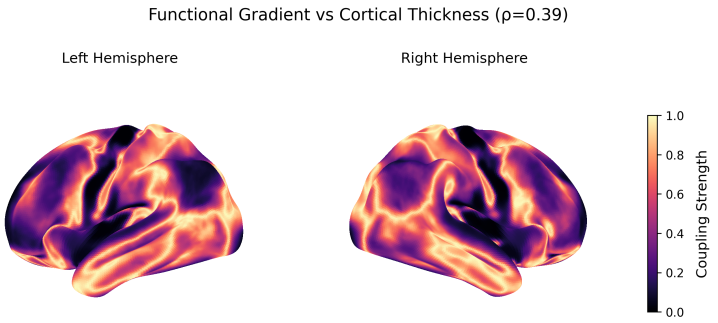

Figure A 19: Functional Gradient v.s Cortical Thickness Coupling Brain Map

Figure A 19 shows the coupling score of the moderate positive relationship between Cortical Thickness and Functional Gradient with $\rho = 0.39$. The brain maps have a slight positive trend in certain regions of the brain.

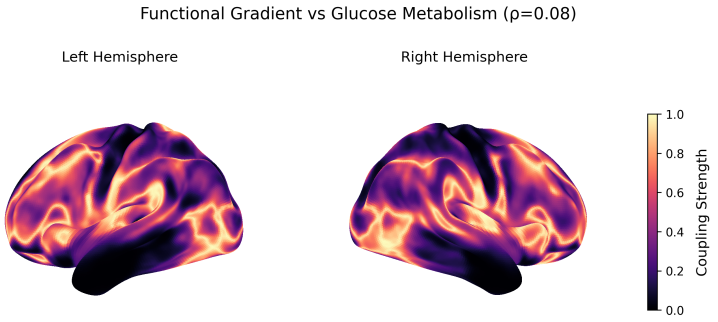

Figure A 20: Functional Gradient v.s Glucose Metabolism Coupling Brain Map

Figure A 20 shows the coupling score of the almost non-existent relationship between Glucose Metabolism and Functional Gradient with $\rho = 0.08$. There are no spatial patterns or relationship between these two brain maps.

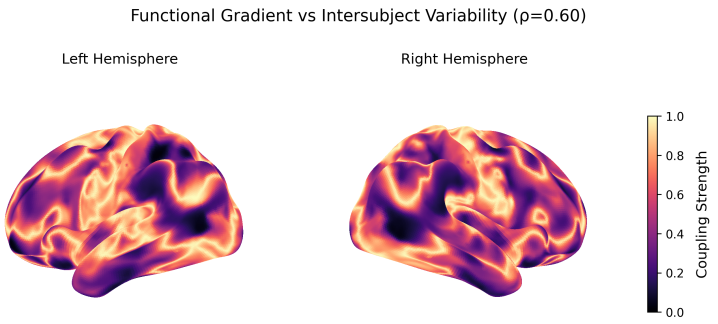

Figure A 21: Functional Gradient v.s Intersubject Variability Coupling Brain Map

Figure A 21 shows the coupling score of the strong positive relationship between Intersubject Variability and Functional Gradient with $\rho = 0.60$. The brain maps are highly tethered.

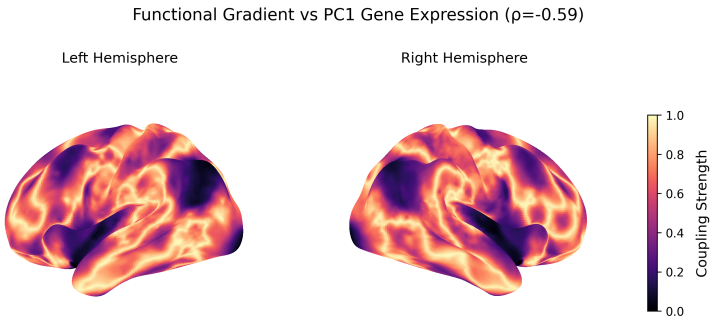

Figure A 22: Functional Gradient v.s PC1 Gene Expression Coupling Brain Map

Figure A 22 shows the coupling score of the strong negative relationship between PC1 Gene Expression and Functional Gradient with ρ = -0.59. The brain maps are mutually exclusive and are inversely tethered.

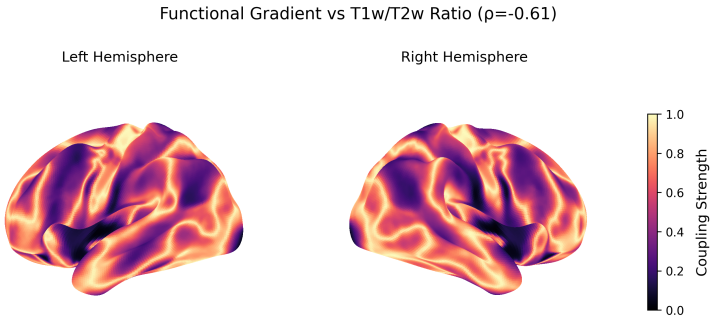

Figure A 23: Functional Gradient v.s T1W/T2W Ratio Coupling Brain Map

Figure A 23 shows the coupling score of the strong negative relationship between T1W/T2W Ratio and Functional Gradient with ρ = -0.61. The brain maps are mutually exclusive and are inversely tethered.

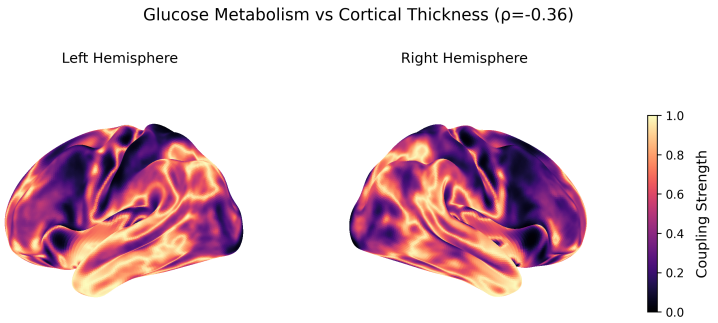

Figure A 24: Glucose Metabolism v.s Cortical Thickness Coupling Brain Map

Figure A 24 shows the coupling score of the moderate negative relationship between Glucose Metabolism and Cortical Thickness with ρ = -0.36. The brain maps are slightly related and inversely tethered.

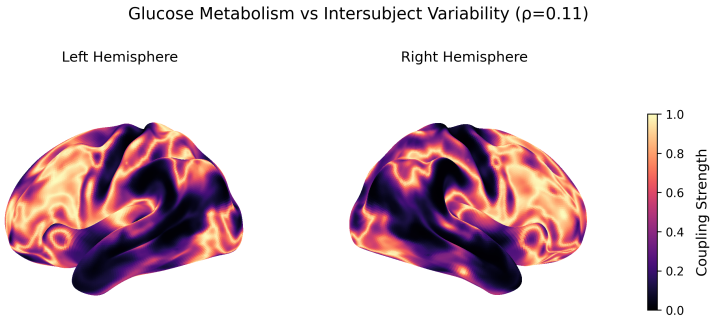

Figure A 25: Glucose Metabolism v.s Intersubject Variability Coupling Brain Map

Figure A 25 shows the coupling score of the weak positive relationship between Glucose Metabolism and Intersubject Variability with ρ = 0.11. The spatial patterns between these brain maps are independent.

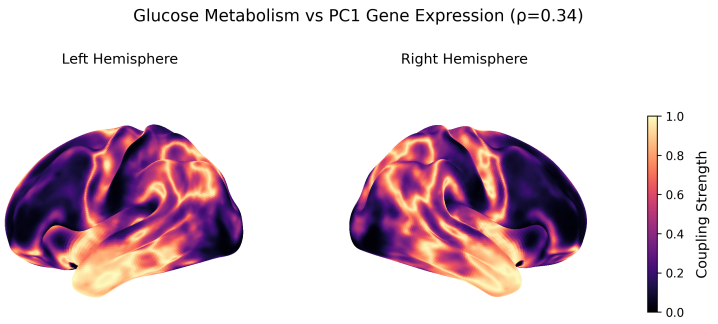

Figure A 26: Glucose Metabolism v.s PC1 Gene Expression Coupling Brain Map

Figure A 26 shows the coupling score of the moderate positive relationship between Glucose Metabolism and PC1 Gene Expression with $\rho = 0.34$. There is a general positive global trend between these brain maps with higher tethering scores in certain regions.

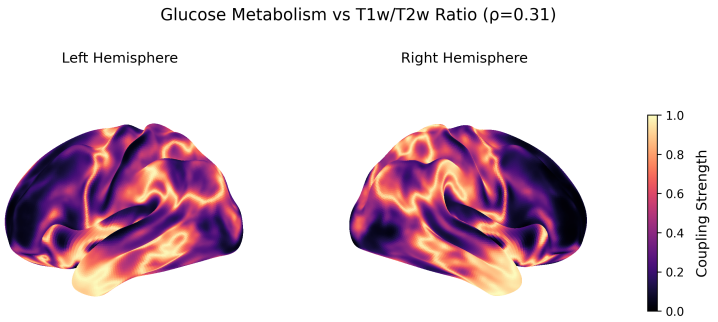

Figure A 27: Glucose Metabolism v.s T1W/T2W Ratio Coupling Brain Map

Figure A 27 shows the coupling score of the moderate positive relationship between Glucose Metabolism and T1W/T2W Ratio with $\rho = 0.31$. There is a general positive global trend between these brain maps with higher tethering scores in certain regions.

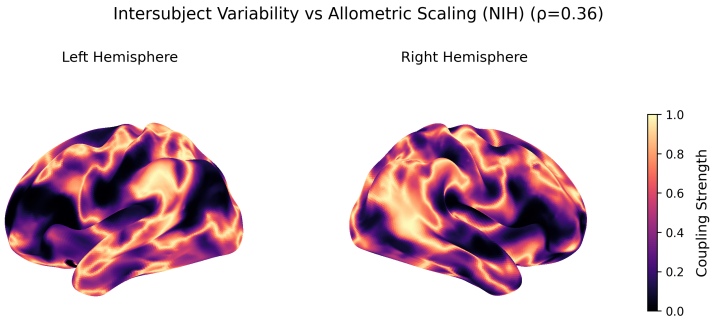

Figure A 28: Intersubject Variability v.s Allometric Scaling (NIH) Coupling Brain Map

Figure A 28 shows the coupling score of the moderate positive relationship between Intersubject Variability and Allometric Scaling (NIH) with $\rho = 0.36$. There is a general positive global trend between these brain maps with higher tethering scores in certain regions.

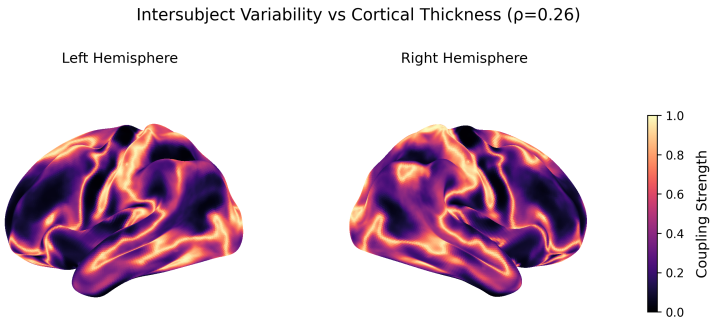

Figure A 29: Intersubject Variability v.s Cortical Thickness Coupling Brain Map

Figure A 29 shows the coupling score of the weak positive relationship between Cortical Thickness and Intersubject Variability with $\rho = 0.26$. The brain maps have no spatial patterns.

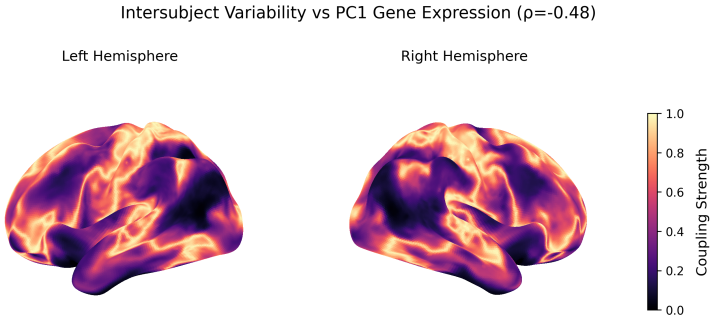

Figure A 30: Intersubject Variability v.s PC1 Gene Expression Coupling Brain Map

Figure A 30 shows the coupling score of the moderate negative relationship between Intersubject Variability and PC1 Gene Expression with ρ = -0.48. There is an general inverse relationship between these brain maps.

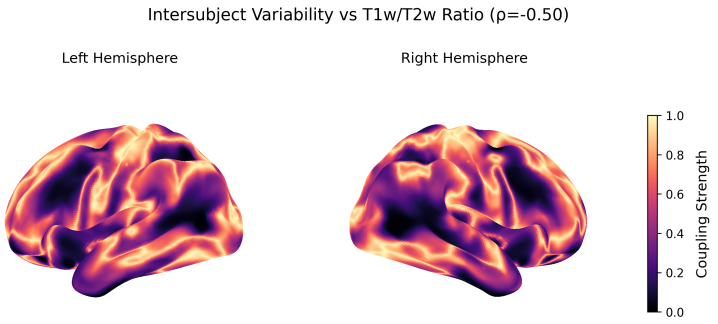

Figure A 31: Intersubject Variability v.s T1W/T2W Ratio Coupling Brain Map

Figure A 31 shows the coupling score of the moderate negative relationship between Inter-subject Variability and T1W/T2W Ratio with ρ = -0.5. The complex relationship results in an inverse global trend.

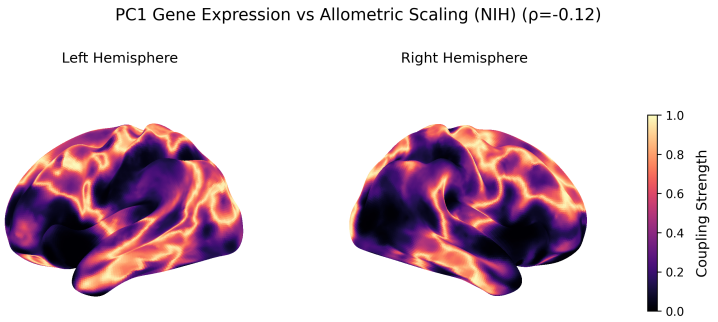

Figure A 32: PC1 Gene Expression v.s Allometric Scaling (NIH) Coupling Brain Map

Figure A 32 shows the coupling score of the weak negative relationship between Allometric Scaling NIH and PC1 Gene Expression with ρ = -0.12. The brain maps are spatially independent.

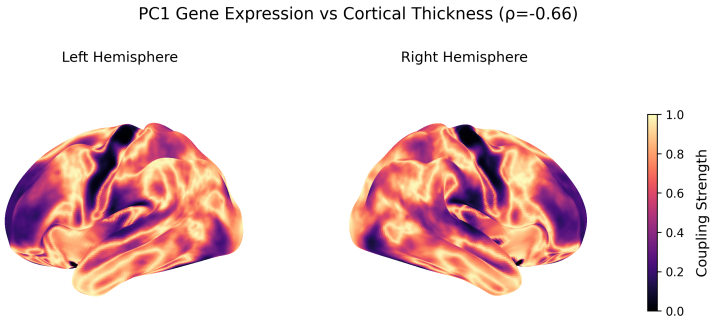

Figure A 33: PC1 Gene Expression v.s Cortical Thickness Coupling Brain Map

Figure A 33 shows the coupling score of the strong negative relationship between Cortical Thickness and PC1 Gene Expression with ρ = -0.66. The brain maps are mutually exclusive, but tightly tethered.

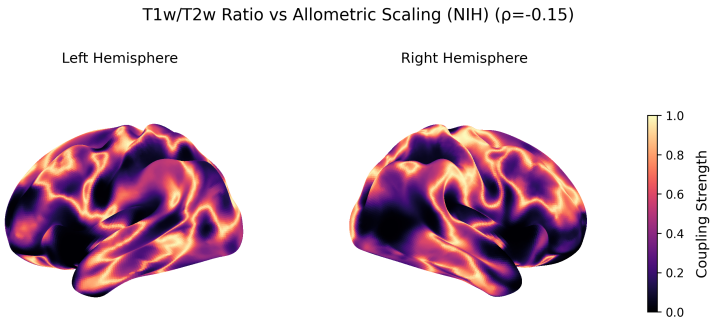

Figure A 34: T1W/T2W Ratio v.s Allometric Scaling (NIH) Coupling Brain Map

Figure A 34 shows the coupling score of the weak negative relationship between Allometric Scaling NIH and T1W/T2W Ratio with ρ = -0.15. The spatial patterns are independent between brain maps with no relationship.

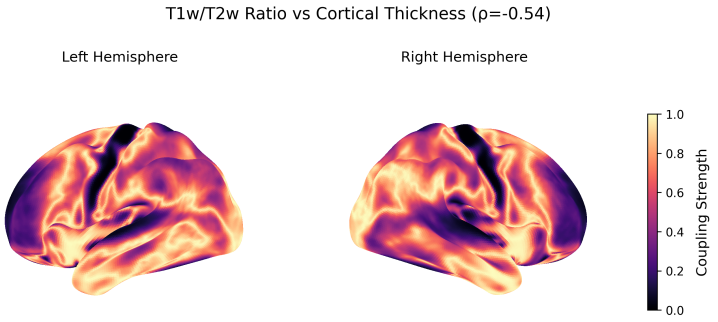

Figure A 35: T1W/T2W Ratio v.s Cortical Thickness Coupling Brain Map

Figure A 35 shows the coupling score of the strong negative relationship between Cortical Thickness and T1W/T2W Ratio with ρ = -0.54. The brain maps have a tethered, mutually exclusive relationship.